

# Validation of Relativistic DFT Approaches to the Calculation of NMR Chemical Shifts in Square-Planar Pt<sup>2+</sup> and Au<sup>3+</sup> Complexes

Tomasz Pawlak,<sup>†,§,||</sup> Markéta L. Munzarová,<sup>\*,†,‡</sup> Leszek Pazderski,<sup>||</sup> and Radek Marek<sup>\*,†,‡</sup>

<sup>†</sup>National Center for Biomolecular Research, Faculty of Science and <sup>‡</sup>Central European Institute of Technology (CEITEC), Masaryk University, Kamenice 5/A4, CZ-62500 Brno, Czech Republic

<sup>§</sup>Center of Molecular and Macromolecular Studies, Polish Academy of Sciences, Sienkiewicza 112, PL-90363 Łódź, Poland

<sup>||</sup>Faculty of Chemistry, Nicholas Copernicus University, Gagarina 7, PL-87100 Toruń, Poland

 Supporting Information

**ABSTRACT:** Recently implemented hybrid density functional methods of calculating nuclear magnetic shielding using the two-component zeroth-order regular approximation approach (*J. Phys. Chem. A* **2009**, *113*, 11495) have been employed for a series of compounds containing heavy transition-metal atoms. These include Pt<sup>2+</sup>, Pd<sup>2+</sup>, and Au<sup>3+</sup> organometallics and metal complexes with azines, some of which exhibit interesting biological and catalytic activities. In this study we investigate the effects of geometry, exchange–correlation functional, solvent, and scalar relativistic and spin–orbit corrections on the nuclear magnetic shielding—mainly for <sup>13</sup>C and <sup>15</sup>N atoms connected to a heavy-atom center. Our calculations demonstrate that the B3LYP method using effective core potentials and a cc-pwCVTZ-PP/6-31G\*\* basis set augmented with the polarizable continuum model of the dimethylsulfoxide solvent provides geometries for the complexes in question which are compatible with the experimental NMR results in terms of both the trends and the absolute values of the <sup>13</sup>C shifts. The important role of the exact exchange admixture parameter for hybrid functionals based on B3LYP and PBE0 is investigated systematically for selected Pt<sup>2+</sup> and Au<sup>3+</sup> complexes. The <sup>13</sup>C and <sup>15</sup>N NMR chemical shifts are found to be best reproduced by using a B3LYP or PBE0 approach with 30% and 40–50% exact exchange admixtures for the Pt<sup>2+</sup> and Au<sup>3+</sup> complexes, respectively. The spin–orbit contributions to the <sup>15</sup>N NMR chemical shifts reflect metal–ligand bonding that is much more ionic for the Au<sup>3+</sup> than for the Pt<sup>2+</sup> complex. Finally, an optimized density functional method is applied to a series of transition-metal complexes to estimate the scope and the limitations of the current approach.

## 1. INTRODUCTION

Azine ligands are known to coordinate with transition-metal ions, such as Pd<sup>2+</sup>, Pt<sup>2+</sup>, and Au<sup>3+</sup>. Many of these coordination compounds exhibit noticeable biological activities or catalytic properties.<sup>1–3</sup> Cytotoxicity in particular has been reported for neutral Pd<sup>2+</sup> and Pt<sup>2+</sup> chloride compounds (e.g., [Pt(2ppy\*)-(DMSO)Cl], **1**; [Pd(2ppy\*)NH<sub>3</sub>Cl]),<sup>4–6</sup> for their bromide and iodide analogs, for cations of the general structure [Pt(2ppy\*)-(LL)]<sup>+</sup>,<sup>7</sup> and for [Au(2ppy\*)Cl<sub>2</sub>, **2**]<sup>8,9</sup> and its analogs,<sup>10,11</sup> wherein 2ppy\* denotes 2-phenylpyridine (2ppy) that has been deprotonated at C-2' and acts as a chelating ligand (see Chart 1). In addition, [Au(2ppy\*)Cl<sub>2</sub>]<sup>12</sup> and some other related compounds<sup>13–16</sup> have been used as catalysts in organic syntheses.

Many of these coordination compounds have been identified as efficient intercalators of nucleic acids.<sup>1</sup> In order to find the structure–activity relationships of these compounds, it is necessary to characterize their structures in detail.<sup>1</sup> Various experimental techniques, e.g., X-ray diffraction, IR and UV-vis spectroscopy, Raman spectroscopy, and mass spectrometry, are frequently employed for structural studies.

Nuclear magnetic resonance (NMR) spectroscopy represents one of the most powerful techniques for characterizing molecular and supramolecular structures both in solution and in the solid state.<sup>17</sup> The NMR chemical shift is very sensitive and is probably the most widely employed NMR probe. Its isotropic value, typically measured in solution, as well as the principal components of the

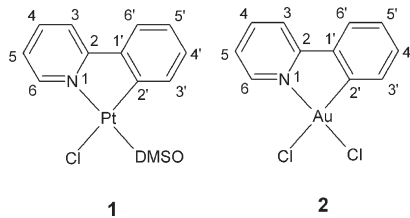
chemical-shift tensor determined for solid samples is derived from the distribution of the electron density surrounding the investigated nucleus. In principle, several nuclei can be employed in NMR studies of transition-metal complexes with heterocyclic ligands.<sup>18</sup> The relative importance of individual effects (e.g., substitution, environment) on a particular chemical shift can be decoded by means of quantum chemical methods.<sup>19</sup>

Density functional theory (DFT) currently represents an efficient compromise between accuracy and the requirements of the computer for calculating NMR chemical shifts. It is frequently used for calculations involving small to medium size molecules or molecular assemblies. However, several physical effects must be taken into account. First, compounds containing transition metals must be treated using methods that cover electron correlation. Second, if the aim is to reproduce or predict the NMR data of condensed phases, solvent or crystal effects must be included.<sup>20</sup> Third, the choice of an appropriate reference compound is crucially important. Typically, secondary reference compounds are selected in order to eliminate the systematic errors arising due to the limitations of the currently used density functionals. Last, but not least, a theoretical description of the structures and spectral properties of compounds containing

**Received:** May 31, 2011

**Published:** November 08, 2011

**Chart 1. Structures and Atom Numbering for Compound 1, *trans*(*S,N*)-[Pt(2-ppy\*)](DMSO)Cl] and Compound 2, [Au(2ppy\*)Cl<sub>2</sub>]**



heavy elements requires the inclusion of relativistic effects,<sup>21</sup> this is particularly important for NMR parameters.<sup>22,23</sup>

The most exact approach to calculating the NMR parameters of transition-metal complexes is a fully relativistic four-component theory, as implemented, for example, in the ReSpect-MAG<sup>24</sup> or Dirac<sup>25</sup> codes. Very recently, four-component codes have also been employed for calculations involving transition-metal complexes.<sup>26</sup> However, for validating various density functional approaches, the selection of the functionals within the four-component codes is rather limited. Other potentially applicable methods include the effective core potential (ECP) treatment<sup>27</sup> of scalar relativistic (SR) effects as well as the one-component (SR) or two-component inclusion of the SR and spin-orbit (SO) effects within the zeroth-order regular approximation (ZORA).<sup>28–33</sup> Both approaches are employed in this study.

In the present paper, we perform a systematic validation study of DFT approaches to the calculation of the NMR chemical shifts for compounds **1** and **2** (Chart 1). Compound **1** is a well-known platinum complex with square-planar coordination,<sup>34–36</sup> which has been characterized by using single-crystal X-ray diffraction.<sup>37</sup> Compound **2** is a structurally related Au<sup>3+</sup> complex. We began our study with a series of geometry optimizations for molecule **1**. For the resulting structure, we tested several approaches to the calculation of NMR chemical shifts and selected one on the basis of its performance relative to experiment, comparing both the trends and the absolute values of the NMR chemical shifts. The selected NMR approach was then applied to the structures resulting from the various geometry optimizations and the X-ray diffraction results. The trends and the absolute values of the chemical shifts were again checked against the experimental data, and the suitability of the selected geometry was confirmed. Our study was completed with the application of the method to a set of four additional Pt<sup>2+</sup> and Pd<sup>2+</sup> square-planar complexes.

## 2. METHODOLOGICAL DETAILS

The quantum chemical calculations were carried out using the Gaussian03 (G03)<sup>38</sup> and Amsterdam Density Functional 2009 (ADF)<sup>39</sup> codes. For the G03 calculations, the scf = tight keyword was used (convergence to  $10^{-8}$  in the energy and to  $10^{-6}$  in the density matrix). An ultrafine grid with 75 radial shells and 302 angular points was employed. The geometry was always optimized without any symmetry restrictions, but all of the resultant structures possessed a horizontal plane of symmetry (group  $C_s$ ).

**2.1. Experimental Molecular Geometry.** The experimental X-ray geometries for compound **1** (Cambridge Crystallographic Data Center code JISPAD01),<sup>35,40</sup> compound **2** (CCDC code IJAQEP),<sup>9</sup> compound **3** (CCDC code SOXZUA),<sup>41</sup> and compound **5** (CCDC code BPYCPT)<sup>42</sup> were obtained from the CCDC.<sup>43</sup> The geometry for compound **1** was used to calibrate

the methods employed to optimize the molecular geometry (Sections 2.2 and 3.1), where the comparisons are carried out only for the positions of atoms other than hydrogen. The data deposited at the CCDC include the positions of the hydrogens, but the resolution is insufficient for our purposes. Hence, for the purpose of computing chemical shifts, “X-ray geometry” denotes the X-ray coordinates of the atoms other than hydrogen augmented by the coordinates of the hydrogens as optimized by using B3LYP/6-31G\*\*.

**2.2. Calculated Molecular Geometry.** The starting structures for the optimization of the geometry were the X-ray geometries for compounds **1**–**3** and **5**. The geometries of compounds **4** and **6** were calculated de novo. The following theoretical methods were used to optimize the molecular geometry: Hartree–Fock (HF),<sup>44,45</sup> Møller–Plesset perturbation theory to the second order (MP2),<sup>46,47</sup> and three different combinations of DFT exchange and correlation potentials, abbreviated as BLYP, B3LYP, and BHandHLYP. The functionals combine the LYP generalized gradient approximation (GGA) for correlation<sup>48</sup> with three different approximations for exchange, namely the Becke’s GGA for exchange (B),<sup>49</sup> the Becke’s three-parameter hybrid functional (B3, this includes 20% of exact exchange),<sup>50</sup> and the “half-and-half” hybrid incorporating as much as 50% of exact exchange.<sup>51</sup> The aforementioned methods were chosen for the following reasons: The B3LYP method has often been reported to perform favorably in comparison with experimental and CCSD(T) structural data.<sup>52</sup> The BLYP and BHandHLYP methods have been used to see the impact of the inclusion of exact exchange on the structural data. The HF method has been included as the most extreme method on the scale BLYP→B3LYP→BHandHLYP→HF. The MP2 method was a natural choice because it usually agrees well with the experimental data for the geometries of 4d and 5d species provided that relativistic effects are taken into account.<sup>52</sup>

The relativistic effective core potentials (ECPs) and basis sets employed for platinum were: ECP60MDF with a 7s,7p,6d,3f,2g correlation consistent orbital basis,<sup>53</sup> ECP60MWB with a 6s,5p,3d,2f,1g orbital basis,<sup>54–56</sup> and Lanl2dz with a 3s,3p,2d orbital basis.<sup>57–59</sup> In the two abbreviations of the form ECP $n$ XY,  $n$  is the number of core electrons which are replaced by the pseudopotential, X denotes the reference system used to generate the pseudopotential (X = M: neutral atom), and Y stands for the theoretical level of the reference data (Y = Dirac–Fock (DF): relativistic, Y = Wood–Boring (WB): quasirelativistic). Lanl2dz is an acronym that stands for Los Alamos National Laboratory 2 double- $\zeta$  (density functional theory). The motive for selecting the ECPs was the generally recognized good performance of the Stuttgart–Cologne MDF and MWB pseudopotentials. The older Lanl2dz pseudopotential was tested because it is very often used in calculations that augment experimental NMR data. The orbital basis sets employed are those recommended for use with the ECPs.

The relativistic ECP ECP60MDF was employed for gold as well, while ECP28MDF (with a correlation consistent cc-pwCVTZ-PP orbital basis) was used for palladium. For nonmetal atoms we tested the Pople bases 6-31G\*, 6-31G\*\*, and 6-311G\* (only the 6-31G\*\* data are shown below).<sup>60–62</sup> The nonmetal basis sets were chosen based on our previous experience with the influence of the size of the basis set on the geometrical parameters. The resulting molecular structures were reoptimized using the polarizable continuum model (PCM) of the solvent. Dimethylsulfoxide (DMSO) was used as the solvent with the following standard parameters: a dielectric constant  $\epsilon$  of 46.7, a molecular

volume of  $70.94 \text{ \AA}^3$ , a numerical density of  $0.00849 \text{ \AA}^{-3}$ , and a radius of the solvent molecule of  $2.455 \text{ \AA}$ .<sup>63,64</sup> Each stationary point was characterized by calculating the harmonic vibration frequencies.

To evaluate the effects of crystal packing on the molecular geometry, we performed a B3LYP optimization (ECP60MDF/6-31G\*\*) of a single molecule of compound 1 surrounded by eight neighboring molecules adopting a topological arrangement that has been characterized by using X-ray diffraction (see Supporting Information). In other words, only the central molecule of this cluster of nine molecules was relaxed.

**2.3. Experimental NMR Chemical Shifts.** The  $^1\text{H}$ ,  $^{13}\text{C}$ , and  $^{15}\text{N}$  NMR chemical shifts discussed in this contribution were measured in dimethylsulfoxide ( $\text{DMSO}-d_6$ ) solution. The  $^1\text{H}$  and  $^{15}\text{N}$  NMR chemical shifts had been reported previously (see footnotes to the tables). The  $^{13}\text{C}$  NMR data were measured as part of this work and were assigned by using the standard 2D  $^1\text{H}$ – $^{13}\text{C}$  NMR correlation techniques, gradient-selected heteronuclear single-quantum correlation (gs-HSQC)<sup>65</sup> and gradient-selected heteronuclear multiple-bond correlation (gs-HMBC).<sup>66,67</sup> The  $^1\text{H}$  and  $^{13}\text{C}$  NMR chemical shifts are reported relative to tetramethylsilane and the  $^{15}\text{N}$  NMR chemical shifts relative to liquid ammonia.<sup>68,69</sup>

**2.4. Nuclear Magnetic Shielding—G03.** The selected geometry was used to calculate the nuclear magnetic shielding by means of DFT and ab initio (HF and MP2) methods using the gauge including atomic orbitals (GIAO) approach.<sup>70–72</sup> We tested the BLYP, B3LYP, and BHandHLYP functionals previously employed to optimize the geometry. We also tested three further combinations of exchange and correlation potentials, abbreviated as BP86, PW91, and PBE0. The first combines Becke's GGA for exchange<sup>49</sup> with the P86<sup>73,74</sup> GGA for correlation. The second uses both the exchange and the correlation parts of the PW91 functional.<sup>75–77</sup> The third is the hybrid functional of Perdew, Burke, and Ernzenhof.<sup>78,79</sup> Two basis sets were used for platinum: cc-pwCVTZ-PP (with relativistic ECP ECP60MDF) and Fægri-III<sup>80,81</sup> (FIII) based on the primitive exponents of Fægri<sup>82</sup> and contracted as well as polarized similarly to the IGLO-III basis set.<sup>83</sup> An optimized basis for light atoms (IGLO-III-UT3, cf. below) was employed. The NMR calculations were performed in vacuo (on an in vacuo optimized geometry) and also using the PCM solvent model (on a PCM reoptimized geometry).

**2.5. Nuclear Magnetic Shielding—ADF.** All GIAO shielding calculations in ADF were performed using the polarized valence triple- $\zeta$  (TZP) basis set from the standard ADF library along with, first, the local density approximation, employing the exchange potential<sup>84</sup> combined with the correlation potentials due to Perdew and Wang (PW92)<sup>85</sup> and to Vosko, Wilk, and Nusair (VWN).<sup>86</sup> Second, we employed the GGA functionals BP86, PW91, and BLYP described above and Keal–Tozer functionals KT1 and KT2<sup>87</sup> which had been optimized for the calculation of chemical shifts. Finally, the hybrid functionals B3LYP, BHandHLYP, and PBE0 were employed. For the functionals B3LYP and PBE0, we systematically investigated the influence of the exact exchange admixture (0–50%) on the nuclear shielding. The latter study was done at the nonrelativistic level using the conductor-like screening (COSMO)<sup>88,89</sup> approach for the DMSO solvent as implemented in ADF<sup>90</sup> and at the ZORA-SO relativistic level using COSMO.

**2.6. Calculated NMR Chemical Shifts.** The choice of the reference compound can help to reduce systematic errors in the DFT calculation of chemical shifts. In this study, we selected

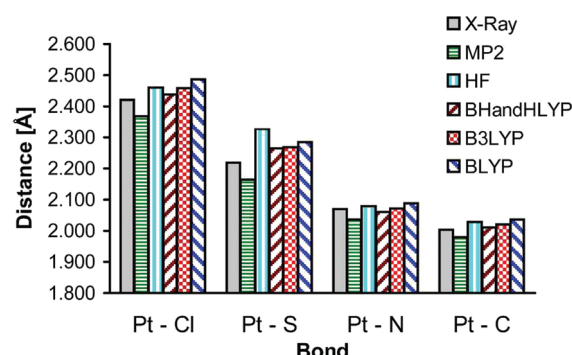


**Figure 1.** Interatomic distances from the platinum center for compound 1, optimized using different functionals with ECP60MDF/cc-pwCVTZ-PP for Pt and the 6-31G\*\* basis set for light atoms.

benzene as the secondary reference<sup>91</sup> for  $^1\text{H}$  and  $^{13}\text{C}$  NMR (residual benzene- $d_5$  in benzene- $d_6$  for  $^1\text{H}$  NMR:  $\delta = 7.15 \text{ ppm}$ , benzene- $d_6$  for  $^{13}\text{C}$  NMR:  $\delta = 127.8 \text{ ppm}$ ), and pyridine in  $\text{DMSO}-d_6$  as the secondary reference for  $^{15}\text{N}$  NMR ( $\delta = 316.9 \text{ ppm}$  relative to liquid ammonia).<sup>68,69,92</sup> The chemical shifts  $\delta_i$  were obtained using the equation:

$$\delta_i = \sigma_{\text{ref}} - \sigma_i + \sigma_{\text{ref}} \quad (1)$$

where  $\sigma_{\text{ref}}$  is the calculated shielding constant of a given nucleus in the reference compound,  $\sigma_i$  is the calculated shielding constant of the investigated nucleus, and  $\delta_{\text{ref}}$  is the experimental chemical shift of the secondary reference relative to the primary standard.

**2.7. SR and SO Contributions to the Chemical Shift.** The SR contribution to the nuclear shielding was calculated as the difference between the SR-ZORA calculation and the fully non-relativistic calculation in the ADF program. The SR contribution to the chemical shift ( $\Delta_{\text{SR}}$ ) was then calculated as

$$\Delta_{\text{SR}} = \sigma_{\text{SR,ref}} - \sigma_{\text{SR},i} \quad (2)$$

where  $\sigma_{\text{SR,ref}}$  is the SR contribution to the nuclear shielding constant in the reference compound and  $\sigma_{\text{SR},i}$  is the SR contribution to the nuclear shielding constant of the investigated nucleus. Similarly, the SO contribution to the chemical shift was calculated as

$$\Delta_{\text{SO}} = \sigma_{\text{SO,ref}} - \sigma_{\text{SO},i} \quad (3)$$

where  $\sigma_{\text{SO,ref}}$  is the SO contribution to the nuclear shielding constant in the reference compound and  $\sigma_{\text{SO},i}$  is the SO contribution to the nuclear shielding constant of the investigated nucleus.

**2.8. Visualizations.** The highest molecular orbitals (MOs) relevant for the  $\Delta_{\text{SO}}$  contribution are visualized in Figures 10 and 11 by using the Molekul program.<sup>93</sup>

### 3. RESULTS AND DISCUSSION

**3.1. Geometries of Compounds 1 and 2.** A series of ab initio and DFT geometry optimizations were performed for compound 1 as characterized by two well-resolved X-ray structures in order to find a suitable computational method for optimizing the structures of complexes 2–5. In Figure 1, the resulting geometries are compared to the JISPAD01 structure (low-temperature structure, more symmetric crystal, lower value of  $R_{\text{int}}$ , and lower residual electron density as compared to the JISPAD structure) in terms of the metal–ligand bond lengths.

The comparison of gas-phase optimized structures and the X-ray geometries obtained for a crystal may appear questionable since crystal-packing effects can, in principle, influence bond lengths substantially. In order to estimate the influence of the crystal packing on the geometry of complex **1**, we performed a B3LYP optimization (with the same parameters as for the other optimizations) of a single molecule of **1** surrounded by its eight nearest neighbors (for atomic coordinates, see Supporting Information). The starting structure was the X-ray geometry of the nine molecules, and only the central molecule of the cluster was relaxed. The resulting bond lengths are given in Table S1, Supporting Information. Compared to the gas-phase optimized counterpart, the bond lengths within the embedded molecule varied by 0.03 Å for the Pt–Cl bond, and by only 0.01 Å or even less for the Pt–S, Pt–N, and Pt–C bonds. Thus, for the Pt–S, Pt–N, and Pt–C bonds, the crystal packing effects turn out to be negligible, and the corresponding bond lengths obtained from the X-ray structures can serve as the standards for evaluating the suitability of various methods of obtaining structures. A comparative calculation showed that the effect of using the structure optimized in the crystal embedding instead of the gas-phase structure results in changes in the chemical shift of 1.3 ppm for N-1, 2.5 ppm for C-2', and 0.5 ppm or less for the remaining atoms. These numbers represent the maximum order of accuracy which can be expected for a comparison between the chemical shielding computed based on X-ray geometry and the NMR shifts obtained experimentally in solution, as presented later in this work.

The metal–carbon, metal–nitrogen, and metal–sulfur bond lengths for complex **1** are obviously best reproduced by the hybrid density functional approaches B3LYP and BHandHLYP. The distances shorten with increasing exact exchange admixture in the density functional; this is most apparent for the Pt–Cl and Pt–S bonds. In agreement with earlier findings,<sup>94</sup> the HF method itself, however, significantly overestimates the Pt–S bond length, while MP2 underestimates all metal–ligand distances. Of the two suitable hybrid density functionals, we have selected the well-established B3LYP approach to the geometry for the following calculations of the NMR shielding constants.

For comparative purposes, we have also performed a series of geometry optimizations employing the ZORA approach. The results, cf. Table S1, Supporting Information, reveal that for the Pt–Cl, Pt–N, and Pt–C bonds, the ZORA bond lengths are 0.01–0.02 Å longer than the ECP MDF bond lengths, while the Pt–S bond length stays approximately constant. The ZORA-SO bond lengths differ from the ZORA bond lengths by less than 0.01 ppm, i.e., the effect of the SO coupling on the geometry is negligible.

In computational studies supplementing routine NMR investigations of transition-metal complexes,<sup>36,95,96</sup> the B3LYP optimization of the geometry is frequently performed with the large-core Lanl2dz effective core potential available in Gaussian. It is employed despite persuasive theoretical results that demonstrate that large-core ECPs are insufficient for both the structures and the NMR parameters and indicate that small-core and relativistic ECPs must be used instead.<sup>97,98</sup> To evaluate the effect of the particular pseudopotential on the geometry, we performed a simple comparative study using the B3LYP optimizations with the small-core quasirelativistic MWB ECP and the large-core Lanl2dz ECP, using the well-established small-core relativistic MDF ECP as reference. The MWB and Lanl2dz ECPs produce Pt–N and Pt–C bond distances that are quite close to those

**Table 1.** Interatomic Distances (in Å) around the Platinum Center in Compound **1** Calculated on an in Vacuo Optimized Geometry Using Various Relativistic ECPs and Basis Sets

	Pt–Cl	Pt–S	Pt–N	Pt–C
MDF <sup>a</sup>	2.458	2.268	2.072	2.021
MWB <sup>b</sup>	2.469	2.277	2.074	2.020
LA <sup>c</sup>	2.508	2.322	2.071	2.020

<sup>a</sup> Geometry optimized using B3LYP/ECP60MDF/cc-pwCVTZ-PP+6-31G\*\*. <sup>b</sup> Geometry optimized using B3LYP/ECP60MWB/ECP60MWB+6-31G\*\*. <sup>c</sup> Geometry optimized using B3LYP/Lanl2dz/Lanl2dz+6-31G\*\*.

given by the reference MDF (Table 1). However, this is not true for the Pt–Cl and Pt–S bonds, where Lanl2dz produces distances which are 0.04–0.05 Å greater than those given by MDF. In addition, the differences between experiment and theory for these two bonds are twice as large for the Lanl2dz ECP (ca. 0.1 Å) as for the Stuttgart ECPs (ca 0.05 Å). Although one might consider these differences for Pt–Cl and Pt–S bonds to be relatively unimportant in a <sup>13</sup>C and <sup>15</sup>N NMR study, the opposite is true due to the indirect trans-substituent effects of the chlorine and sulfur atoms on the nuclear shieldings of <sup>13</sup>C and <sup>15</sup>N.

The structure of complex **2** was optimized using the BLYP, B3LYP, BHandHLYP, HF, and MP2 methods as described in the Methodological Details Section. The resulting metal–ligand bond lengths are compared to the available X-ray data in Figure S1, Supporting Information. As for complex **1**, the MP2 bond lengths are the shortest, while, contrary to complex **1**, the BLYP bond lengths are in all cases the longest. A comparison with experiment might indicate that the BHandHLYP bond lengths are “best” for the Au–Cl bonds, while the MP2 bond lengths are “best” for the Au–C2' and Au–N bonds. However, since the resolution of the X-ray structure (CCDC code IJAQEP)<sup>35</sup> is relatively poor and a test NMR calculation on the X-ray structure gave meaningless results (cf. below), we consider the X-ray structure to be useless for comparing the bond lengths.

**3.2. Nuclear Magnetic Shieldings for Compounds **1** and **2**.** Below, we perform a systematic study for compound **1** in order to identify the optimum method for calculating the NMR chemical shifts. The method is characterized by the level of calculation of the nonrelativistic nuclear magnetic shielding (we test various basis sets and density functionals there), the inclusion of the surroundings (gas-phase calculation, continuum model), and the treatment of relativistic effects (nonrelativistic, SR, or including both SR and SO effects). When comparing the computed and experimental data, we try, where possible, to decouple these individual effects by determining atoms for which some of the influences could prove negligible. Furthermore, we use the additivity of the individual effects when this can be demonstrated. Finally, we focus on trends in the nuclear magnetic shielding within the whole molecule. This enables us to judge the quality of the description globally, which is always more reliable than attempting to “fit” the individual shifts to experiment as closely as possible.

**3.2.1. Basis for Nonmetal Atoms: A Convergence Study for Compound **1**.** The convergence of the standard IGLO-III<sup>83</sup> basis set (also known as Huzinaga–Kutzelnig HIII)<sup>99</sup> for calculating the chemical shifts of the light atoms C-2' and N-1 was carefully tested at the SR level. The results are shown in Figure 2. The procedure was done independently for each of the two atoms in the following way: First, the standard IGLO-III was uncontracted

(IGLO-III-U). Second, one extra function was added to each type of angular momentum (*s*, *p*, and *d*) with an exponent three times as large as that already available. (The values of the high exponents have been chosen according to the fact that in variationally optimized bases, the ratio between two successive exponents is approximately constant.<sup>100</sup> Within the IGLO-III basis set, this ratio is close to 3.) The addition of the extra functions was done systematically in three steps (resulting in the bases IGLO-III-UT1, IGLO-III-UT2, and IGLO-III-UT3). Third, three additional diffuse functions were continually added to each angular momentum type with an exponent one-third as large as that already available, resulting in the bases UT3\_D1, UT3\_D2, and UT3\_D3. Finally, one extra polarization function of *f* type was added from the cc-pVQZ basis set.<sup>101</sup> As demonstrated in

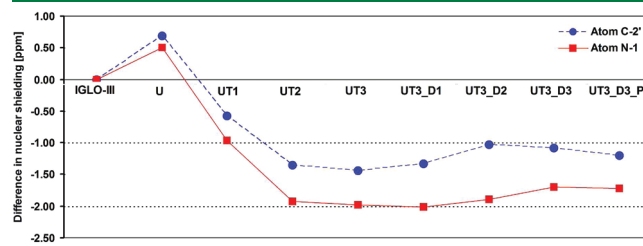


**Figure 2.** Convergence of the IGLO-III basis set (B3LYP with ECP60MDF/cc-pwCVTZ-PP for Pt and IGLO-III for light atoms) for atoms N-1 and C-2' in compound 1. U, uncontracted; UT1, uncontracted with one set of tight functions added, etc.; UT3\_D1, uncontracted with three sets of tight functions and one set of diffuse functions, etc.; and UT3\_D3\_P, including one additional *f* polarization function. The differences in the nuclear magnetic shielding relative to IGLO-III are plotted on the *y* axis.

Figure 2, going from the IGLO-III to the IGLO-III-UT3 basis decreases the nuclear shieldings of C-2' and N-1 by ca. 1.5 and 2 ppm, respectively. Augmenting the basis further with the diffuse and polarization functions increases the nuclear shieldings by ca. 0.3 ppm. Thus, we consider the “middle-size” IGLO-III-UT3 as a very good compromise between cost and accuracy and apply it in all subsequent calculations.

For comparative purposes, we have also tested a few Jensen's pcS-*n* bases<sup>102</sup> for the light atoms, namely pcS-2, pcS-3, and pcS-4, of which the pcS-3 basis is closest in size to our IGLO-III-UT3 basis. The nuclear magnetic shieldings obtained with pcS-3 are ca. 0.5 ppm more negative than those calculated by using the IGLO-III-UT3, whereas the pcS-2 and pcS-4 shielding constants of C-2' and N-1 lie within 1.2 ppm of those calculated by using pcS-3.

**3.2.2. NR Terms and Solvent Corrections (SOLV): B3LYP Results for 1.** The relatively most important solvent effects on the NMR chemical shift can be expected for the hydrogen atoms, which are located in the outer sphere of the molecule and are thus most susceptible to potential solute–solvent interactions. This is indeed evident from Table 2, where the *in vacuo* results, the PCM results (obtained with G03), and the COSMO results (obtained with ADF) are summarized and compared.  $\Delta\delta_{\text{solv}}$  is defined as  $\Delta\delta_{\text{solv}} = \delta_{\text{solv}} - \delta_{\text{in vacuo}}$ , where  $\delta_{\text{solv}}$  and  $\delta_{\text{in vacuo}}$  denote the chemical shifts resulting from the geometry optimization and the chemical shift calculation with and without the implicit solvent model, respectively. The relative influence of the implicit solvent is on average 8% for the hydrogens but as little as 2% for the carbons and the nitrogen. Since the root-mean-square deviation (RMSD) values for the chemical shifts of the hydrogen atoms after the inclusion of solvent effects are 3–4 times smaller than those calculated in *vacuo*, the inclusion of the implicit solvent

**Table 2. Analysis of Implicit Solvent Effects ( $\Delta\delta_{\text{solv}}$  in ppm) for Compound 1<sup>a</sup>**

atom	$\delta_{\text{G03,NR}}$ (in <i>vacuo</i> ) <sup>b</sup>	$\delta_{\text{G03,NR}}$ (PCM) <sup>c</sup>	$\Delta\delta_{\text{solv}}$	$\delta_{\text{ADF,NR}}$ (in <i>vacuo</i> ) <sup>d</sup>	$\delta_{\text{ADF,NR}}$ (COSMO) <sup>e</sup>	$\Delta\delta_{\text{solv}}$
H-3	7.26	7.87	+0.61	7.15	7.75	+0.60
H-4	7.26	7.92	+0.66	7.19	7.83	+0.64
H-5	6.57	7.19	+0.62	6.55	7.17	+0.62
H-6	9.94	9.52	-0.42	9.97	9.43	-0.54
H-3'	8.65	8.52	-0.13	8.64	8.56	-0.08
H-4'	6.95	7.28	+0.33	6.84	7.16	+0.32
H-5'	6.76	7.21	+0.45	6.62	7.11	+0.49
H-6'	7.26	7.82	+0.56	7.11	7.75	+0.64
RMSD	0.64	0.20		0.71	0.24	
N-1	256.3	252.7	-3.6	287.2	282.1	-5.1
C-2	169.3	167.9	-1.4	169.0	166.6	-2.4
C-3	115.1	118.4	+3.3	115.5	119.3	+3.8
C-4	137.4	141.6	+4.2	137.1	141.8	+4.7
C-5	117.7	121.4	+3.7	118.6	123.1	+4.5
C-6	154.2	152.5	-1.7	152.9	151.6	-1.3
C-1'	145.0	147.2	+2.2	145.8	147.7	+1.9
C-2'	184.4	182.2	-2.2	184.1	180.4	-3.7
C-3'	136.8	134.7	-2.1	136.4	134.5	-1.9
C-4'	131.1	130.8	-0.3	130.6	130.8	+0.2
C-5'	123.2	125.3	+2.1	122.9	125.7	+2.8
C-6'	122.2	124.7	+2.5	121.5	124.8	+3.3
RMSD	13.8/3.6 <sup>f</sup>	12.8/1.8 <sup>f</sup>		13.6/3.3 <sup>f</sup>	12.2/1.5 <sup>f</sup>	

<sup>a</sup> All chemical shifts obtained with B3LYP. <sup>b</sup> G03/FIII/IGLO-III-UT3//G03/ECP60MDF/cc-pwCVTZ-PP/6-31G\*\*. <sup>c</sup> G03/FIII/IGLO-III-UT3//PCM//G03/ECP60MDF/cc-pwCVTZ-PP/6-31G\*\*/PCM. <sup>d</sup> ADF/TZP//G03/ECP60MDF/cc-pwCVTZ-PP/6-31G\*\*. <sup>e</sup> ADF/TZP/COSMO//G03/ECP60MDF/cc-pwCVTZ-PP/6-31G\*\*/PCM. <sup>f</sup> RMSD for all carbons/RMSD for all carbons excluding C-2'.

**Table 3.** SR Contributions to the NMR Chemical Shifts ( $\delta$  in ppm) for Complex **1<sup>a</sup>** Calculated Using B3LYP

atom	$\delta_{G03,NR}^b$	$\delta_{G03,SR}^c$	$\Delta_{SR,ECP}$	$\delta_{ADF,NR}^d$	$\delta_{ADF,SR}^e$	$\Delta_{SR,ZORA}$
N-1	252.7	240.4	-12.3	255.2	244.4	-10.8
C-2	167.9	164.0	-3.9	166.6	162.6	-4.0
C-3	118.4	118.1	-0.3	119.3	119.2	-0.1
C-4	141.6	141.9	+0.3	141.8	142.2	+0.4
C-5	121.4	121.6	+0.2	123.1	123.3	+0.2
C-6	152.5	151.2	-1.3	151.6	150.5	-1.1
C-1'	147.2	143.7	-3.5	147.7	144.4	-3.3
C-2'	182.2	173.2	-9.0	180.4	171.8	-8.6
C-3'	134.7	135.4	+0.7	134.5	135.6	+1.1
C-4'	130.8	131.3	+0.5	130.8	131.4	+0.6
C-5'	125.3	124.2	-1.1	125.7	124.7	-1.0
C-6'	124.7	124.3	-0.4	124.8	124.6	-0.2
H-3	7.87	7.83	-0.04	7.75	7.80	+0.05
H-4	7.92	7.87	-0.05	7.83	7.84	+0.01
H-5	7.19	7.20	+0.01	7.17	7.21	+0.04
H-6	9.52	9.36	-0.16	9.43	9.35	-0.08
H-3'	8.52	8.43	-0.09	8.56	8.54	-0.02
H-4'	7.28	7.24	-0.04	7.16	7.17	+0.01
H-5'	7.21	7.11	-0.10	7.11	7.05	-0.06
H-6'	7.82	7.74	-0.08	7.75	7.73	-0.02

<sup>a</sup> Calculations on a structure optimized in PCM, employing DMSO, and using B3LYP/ECP60MDF/cc-pwCVTZ-PP for Pt and 6-31G\*\* for light atoms in the G03 program. <sup>b</sup> NMR chemical shifts calculated using G03/B3LYP/Fægri-III for Pt and IGLO-III-UT3 for light atoms, PCM. <sup>c</sup> G03/B3LYP/ECP60MDF/cc-pwCVTZ-PP for Pt and IGLO-III-UT3 for light atoms, PCM. <sup>d</sup> NMR chemical shifts calculated using ADF/B3LYP/TZP/COSMO. <sup>e</sup> ADF/B3LYP/SR-ZORA/TZP/COSMO.

decidedly improves the model. Indeed, the implicit solvent can be well decoupled from the other theoretical parameters since the influences of the relativistic effects and the density functional on the <sup>1</sup>H NMR chemical shifts are much smaller in our systems (cf. Table 3 and Table S2, Supporting Information). The values calculated by using the PCM and COSMO models are very similar (differences being smaller than 0.12 ppm). We employed the COSMO model as implemented in ADF in the production calculations.

**3.2.3. SR and SO Contributions: Results for Compound **1**.** To determine the importance of the SR effects, we calculated SR chemical shifts in G03 using relativistic ECP (ECP60MDF with the cc-pwCVTZ-PP basis set) along with several pure GGA (BP86, PW91, BLYP) and hybrid GGA (B3LYP and BHandHLYP) functionals. As an alternative, the SR chemical shifts were calculated in the ADF program using the all-electron ZORA (scalar ZORA). The SR correction to the chemical shift ( $\Delta_{SR}$ ) was then calculated as the difference between the SR chemical shift ( $\delta_{SR}$ ) and its non-relativistic counterpart ( $\delta_{NR}$ ):

$$\Delta_{SR} = \delta_{SR} - \delta_{NR} \quad (4)$$

where  $\delta_{SR}$  is the SR chemical shift (G03<sub>ECP</sub> or ADF<sub>ZORA</sub>) and  $\delta_{NR}$  is the nonrelativistic chemical shift calculated using G03 (FIII/IGLO-III-UT3) or ADF (TZP).

The results for both of these approaches ( $\delta_{G03,SR}$  and  $\delta_{ADF,SR}$ ) using the B3LYP functional as an example are summarized in Table 3. Values for the other functionals tested in this study are collected in Table S3, Supporting Information. The results

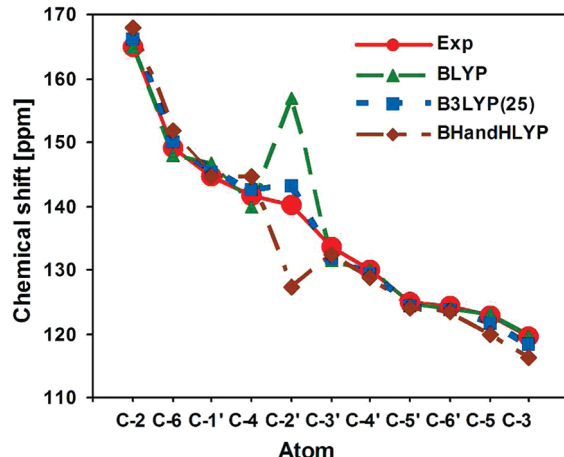


**Figure 3.** Experimental <sup>13</sup>C NMR chemical shifts for compound **1** and those calculated by using BLYP, B3LYP(25), and BHandHLYP functionals (TZP/ZORA-SO/COSMO). A fixed B3LYP optimized structure (ECP60MDF/cc-pwCVTZ-PP for Pt and 6-31G\*\* for light atoms, PCM) was employed for all calculations. The atoms are placed on the x axis according to decreasing experimental NMR chemical shift.

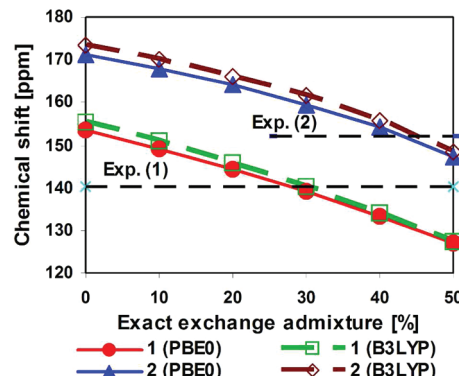


**Figure 4.** NMR chemical shift for C-2' in compounds **1** and **2** as a function of the exact exchange admixture for the PBE0 and B3LYP functionals calculated using the ADF/TZP/ZORA-SO/COSMO approach. Experimental values are shown as dashed lines.

demonstrate excellent agreement between the SR effects covered by relativistic ECP ( $\Delta_{SR,ECP}$ ) and those calculated using the all-electron treatment of the SR ZORA approach ( $\Delta_{SR,ZORA}$ ).

The second significant relativistic contribution is the SO term, which has long been recognized as important for the NMR chemical shift in compounds containing heavy atoms.<sup>103–106</sup> Although the SR and SO contributions are partly self-compensating for some of the carbon and hydrogen atoms, they operate in the same direction for C-2' and N-1 and also leave non-negligible total relativistic corrections ( $\Delta_{SR} + \Delta_{SO}$ ) for C-6, C-1', and C-3'. The influence of the density functional on all of the NR, SR, and SO terms is investigated systematically in Section 3.2.4.

**3.2.4. NR, SR, and SO Terms: Influence of the Density Functional for Compounds **1** and **2**.** Various local density approximation and GGA methods (PW92, VWN, BP86, PW91, BLYP, KT1, KT2) give very similar NR chemical shift values (see Table S2 and Figures S2 and S3, Supporting Information). The chemical shift variation for individual functionals is within 1 ppm for all carbons except C-2' (where it reaches 2.5 ppm) and within 0.05 ppm for

all hydrogens. The effect of the exact exchange admixture is much more significant: Variations for BLYP, B3LYP, and BHandHLYP are within 7 ppm for C-2', 5 ppm for the remaining carbons, and 0.3 ppm for the hydrogens.

The inclusion of SR and SO contributions (Tables S3 and S4, Supporting Information) makes the dependence of the NMR chemical shift on the density functional much more pronounced, especially for the N and C atoms bonded directly to the transition-metal center. The NMR chemical shifts for all of the carbon atoms of compound **1** obtained by the BLYP, B3LYP (with 25% of exact exchange) and BHandHLYP functionals are compared in Figure 3.

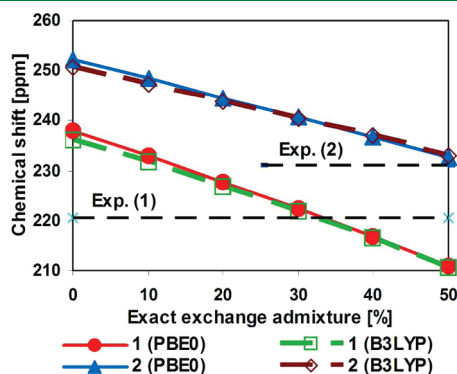


**Figure 5.** NMR chemical shift for N-1 in compounds **1** and **2** as a function of the exact exchange admixture for the PBE0 and B3LYP functionals calculated using the ADF/TZP/ZORA-SO/COSMO approach. Experimental values are shown as dashed lines.

The influence of 50% of exact exchange amounts to only up to 0.3 ppm for the hydrogens (i.e., less than the effect of solvation), cf. Table S5, Supporting Information, but it reaches up to 4 ppm for the carbon atoms. However, for the carbon atom C-2', which is bonded directly to the metal center, the effect is as great as 30 ppm! We note that similar dramatic effects of HF exchange have previously been reported for transition-metal NMR shifts.<sup>107</sup>

The amount of the exact exchange admixture is quantitatively more important than a particular DFT exchange or correlation functional within our testing set. Indeed, the effect of the 0 to 50% exact exchange admixture on N-1 in compound **1** is as large as 32 ppm, while our ZORA-SO results for the PW92, VWN, BP86, PW91, and BLYP functionals (Table S4, Supporting Information) are within 3 ppm for all carbons including C-2' and within 5 ppm for N-1. However, it should be noted that a small dependence on a particular functional can arise due in part to the adiabatic local density approximation employed for the exchange–correlation kernel within the ADF.

Two classes of hybrid functionals have been popular in recent NMR studies: those based on the BLYP and those based on the PBE exchange–correlation functional. In order to validate their performance for our systems in detail, we studied the effect of the exact exchange admixture from 0 to 50% on a 10% grid for both classes (B3LYP and PBE0). At this point, we also introduced compound **2** in the NMR study, in order to compare the two structurally related isoelectronic species. The computed chemical shifts are plotted in Figures 4 and 5 as functions of increasing exact exchange admixture. Obviously, both the C-2' and the N-1 chemical shifts decrease as the exact exchange admixture

**Table 4. NMR Chemical Shifts for Compound 1 Calculated by ADF using PBE0(30)/TZP/ZORA-SO/COSMO with Solvent Effects ( $\Delta\delta_{\text{solv}}$ ) and SR ( $\Delta_{\text{SR}}$ ) and SO ( $\Delta_{\text{SO}}$ ) Contributions Shown Separately**

atom	$\delta_{\text{NR}}$ (in vacuo) <sup>a</sup>	$\Delta\delta_{\text{solv}}$	$\delta_{\text{NR,solv}}$ (COSMO) <sup>b</sup>	$\Delta_{\text{SR}}$	$\delta_{\text{NR,solv}} + \Delta_{\text{SR}}^c$	$\Delta_{\text{SO}}$	$\delta_{\text{NR,solv}} + \Delta_{\text{SR}} + \Delta_{\text{SO}}^c$	expt <sup>e</sup>
N-1	258.5	-5.6	252.9	-12.4	240.5	-18.1	222.4	220.6
C-2	169.3	-2.6	165.1	-4.2	160.9	+3.8	164.7	165.0
C-3	116.4	+3.8	118.7	-0.5	118.2	+0.1	118.3	119.5
C-4	138.7	+4.8	142.0	+0.2	142.2	+0.5	142.7	141.6
C-5	119.6	+4.6	122.6	0.0	122.6	-0.6	122.0	122.8
C-6	154.3	-1.2	151.6	-2.1	149.5	+0.7	150.2	149.2
C-1'	145.6	+1.7	145.8	-3.6	142.2	+1.8	144.0	144.5
C-2'	181.5	-4.2	175.8	-9.0	166.8	-27.7	139.1	140.2
C-3'	137.4	-1.8	134.1	+0.7	134.8	-3.1	131.7	133.5
C-4'	131.6	+0.5	130.6	+0.3	130.9	-1.2	129.7	130.0
C-5'	124.0	+3.0	125.4	-1.3	124.1	+0.4	124.5	124.9
C-6'	122.8	+3.4	124.7	-0.6	124.1	-0.3	123.8	124.3
RMSD	12.8/3.1 <sup>d</sup>		10.8/1.0 <sup>d</sup>		8.2/1.7 <sup>d</sup>		0.9/0.9 <sup>d</sup>	
H-3	7.15	+0.63	7.78	+0.08	7.86	-0.09	7.77	8.14
H-4	7.22	+0.68	7.90	+0.04	7.94	+0.01	7.95	8.12
H-5	6.55	+0.66	7.21	+0.07	7.28	-0.07	7.21	7.50
H-6	9.79	-0.41	9.38	-0.07	9.31	+0.08	9.39	9.48
H-3'	8.59	-0.07	8.52	0.00	8.52	-0.02	8.50	8.21
H-4'	6.83	+0.36	7.19	+0.03	7.22	-0.13	7.09	7.13
H-5'	6.62	+0.53	7.15	-0.03	7.12	0.00	7.12	7.17
H-6'	7.13	+0.67	7.80	0.00	7.80	-0.15	7.65	7.77
RMSD	0.68		0.22		0.19		0.21	

<sup>a</sup> ADF/PBE0(30)/TZP//G03/B3LYP/ECP60MDF/cc-pwCVTZ-PP+6-31G\*\*. <sup>b</sup> ADF/PBE0(30)/TZP/COSMO//G03/B3LYP/ECP60MDF/cc-pwCVTZ-PP+6-31G\*\*/PCM. <sup>c</sup> ADF/PBE0(30)/TZP/ZORA-SO/COSMO//G03/B3LYP/ECP60MDF/cc-pwCVTZ-PP+6-31G\*\*/PCM. <sup>d</sup> RMSD for all carbons/RMSD for all carbons excluding C-2'. <sup>e</sup> Data from reference Pazderski, L.; Pawlak, T.; Sitkowski, J.; Kozerski, L.; Szlyk, E. *Magn. Reson. Chem.* **2009**, 47, 932.

**Table 5.** NMR Chemical Shifts for Compound 2 Calculated by ADF using PBE0(40)/TZP/ZORA-SO/COSMO with Solvent Effects ( $\Delta\delta_{\text{solv}}$ ) and SR ( $\Delta_{\text{SR}}$ ) and SO ( $\Delta_{\text{SO}}$ ) Contributions Shown Separately

atom	$\delta_{\text{NR}}$ (in vacuo) <sup>a</sup>	$\Delta\delta_{\text{solv}}$	$\delta_{\text{NR,solv}}$ (COSMO) <sup>b</sup>	$\Delta_{\text{SR}}$	$\delta_{\text{NR solv}} + \Delta_{\text{SR}}^c$	$\Delta_{\text{SO}}$	$\delta_{\text{NR solv}} + \Delta_{\text{SR}} + \Delta_{\text{SO}}^c$	expt <sup>e</sup>
N-1	258.7	-0.6	258.1	-21.1	237.0	-0.2	236.8	231.1
C-2	168.9	-1.9	167.0	-4.8	162.2	+2.9	165.1	163.9
C-3	116.0	+5.1	121.1	-0.9	120.2	0.0	120.2	122.2
C-4	140.3	+5.2	145.5	+0.4	145.9	+0.3	146.2	143.9
C-5	119.8	+4.3	124.1	+0.1	124.2	-0.6	123.6	125.3
C-6	153.6	-1.7	151.9	-1.6	150.3	-0.4	149.9	148.0
C-1'	143.6	+2.2	145.8	-4.1	141.7	-0.1	141.6	142.9
C-2'	188.4	+9.2	197.6	-27.9	169.7	-15.6	154.1	152.2
C-3'	137.4	-2.8	134.6	-1.3	133.3	-3.1	130.2	130.0
C-4'	132.1	+1.1	133.2	+0.5	133.7	-1.8	131.9	131.6
C-5'	127.7	+2.2	129.9	-1.9	128.0	+0.7	128.7	129.3
C-6'	122.6	+5.4	128.0	-1.1	126.9	-0.7	126.2	126.7
RMSD	11.8/4.6 <sup>d</sup>		13.9/2.5 <sup>d</sup>		5.6/1.9 <sup>d</sup>		1.5/1.4 <sup>d</sup>	
H-3	7.24	+0.61	7.85	+0.10	7.95	-0.08	7.87	8.41
H-4	7.42	+0.67	8.09	+0.03	8.12	+0.01	8.13	8.38
H-5	6.81	+0.57	7.38	+0.08	7.46	-0.12	7.34	7.76
H-6	10.21	-0.85	9.36	-0.15	9.21	+0.12	9.33	9.52
H-3'	8.50	-0.33	8.17	-0.10	8.07	-0.34	7.73	7.81
H-4'	6.90	+0.35	7.25	+0.09	7.34	-0.20	7.14	7.36
H-5'	6.83	+0.55	7.38	-0.02	7.36	-0.02	7.34	7.47
H-6'	7.25	+0.66	7.91	0.00	7.91	-0.26	7.65	7.97
RMSD	0.81		0.30		0.26		0.30	

<sup>a</sup>ADF/PBE0(40)/TZP//G03/B3LYP/ECP60MDF/cc-pwCVTZ-PP+6-31G\*\*. <sup>b</sup>ADF/PBE0(40)/TZP/COSMO//G03/B3LYP/ECP60MDF/cc-pwCVTZ-PP+6-31G\*\*/PCM. <sup>c</sup>ADF/PBE0(40)/TZP/ZORA-SO/COSMO//G03/B3LYP/ECP60MDF/cc-pwCVTZ-PP+6-31G\*\*/PCM. <sup>d</sup>RMSD for all carbons/RMSD for all carbons excluding C-2'. <sup>e</sup>Data from reference Pazderski, L.; Pawlak, T.; Sitkowski, J.; Kozerski, L.; Szlyk, E. *Magn. Reson. Chem.* **2009**, *47*, 932.

increases. Results closest to the experimental data were obtained by the PBE0 functional with 30% of exact exchange, denoted later as PBE0(30) for complex **1** and with the PBE0 functional with 40–50% of exact exchange, denoted later as PBE0(40) and PBE0(50), for complex **2**. The optimum amount of the exact exchange in the density functional thus turns out to be different for the complexes of Pt and Au. This is by no means a unique example of such an observation.<sup>108</sup>

Considering the NMR chemical shifts of all of the atoms, results slightly closer to the experimental values were obtained by using PBE0(30) for **1** (Table 4) and PBE0(40) for **2** (Table 5) as compared to the B3LYP(30) results for **1** (Table S5, Supporting Information) and the B3LYP(40) results for **2** (Table S6, Supporting Information). Here, the number in parentheses stands for the percentage of exact exchange substituted for the DFT exchange. Consequently, the PBE0 functional with 30 or 40% of exact exchange admixture has been employed for comparative purposes on a larger set of compounds, including the Pd<sup>2+</sup> species.

Analysis of the individual NR, SR, and SO contributions to the NMR chemical shift of carbon C-2' in compound **1** reveals that the SR contribution remains practically constant for the various density functionals (see Figure 6). The NR part varies slightly, and the SO part is mainly responsible for any changes in the total chemical shift. The dependence observed for N-1 is similar to that for C-2', with the SR variability slightly increased (Figure 7). These results are fully compatible with those obtained from a SR study and a fully NR study of the influence of the density functional (Tables S2–S4, Supporting Information).

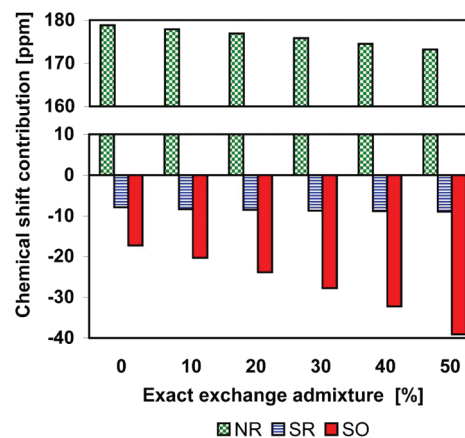


**Figure 6.** NR, SR, and SO contributions to the NMR chemical shift for C-2' in compound **1** calculated by using a PBE0 functional with various amounts of exact exchange.

Interestingly, for compound **2**, the individual contributions to the NMR chemical shift depend differently on the density functional than those calculated for compound **1**. For C-2', the NR part remains constant, the SR contribution varies slightly, and that of SO varies strongly (Figure 8). For N-1, the most constant contribution is surprisingly that of SO, while the NR and SR contributions vary comparably (Figure 9).

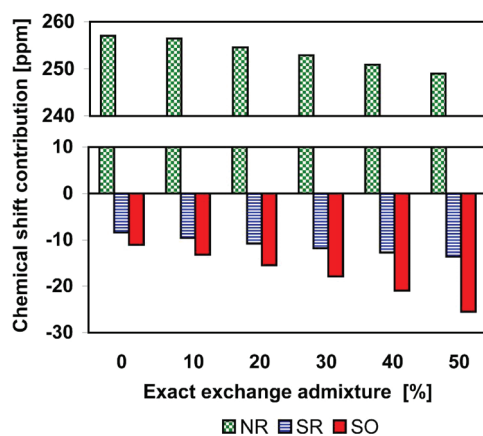


**Figure 7.** NR, SR, and SO contributions to the NMR chemical shift for N-1 in compound **1** calculated by using a PBE0 functional with various amounts of exact exchange.

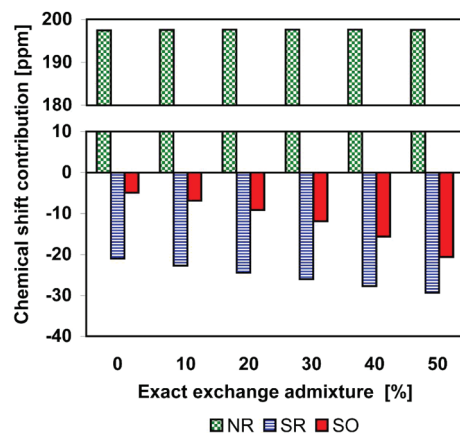


**Figure 8.** NR, SR, and SO contributions to the NMR chemical shift for C-2' in compound **2** calculated by using a PBE0 functional with various amounts of exact exchange.

**3.2.5. Interpretation of the SO Contribution in **1** vs **2**.** In compound **1**, the SO contribution exceeds the SR contribution by a factor of 3 for C-2' and by 1.5 for N-1 (Table 4). In compound **2**, on the contrary, the SR contribution exceeds the SO contribution by a factor of 2 for C-2' and by 2 orders of magnitude for N-1 (-21.1 vs -0.2 ppm, cf. Table 5)! Especially striking is the vanishingly small  $\Delta_{\text{SO}}$  for the  $\text{Au}^{3+}$  complex. The natural localized MO analysis of the Pt/Au–N bond (14% on the metal, 79% on the nitrogen and equivalent s–p hybridization for the nitrogen for both complexes) does not provide any basis for understanding this phenomenon. However, a significant difference in bonding is reflected in the canonical Kohn–Sham MOs.

Already based on qualitative MO considerations, the bonding in complex **1** should be different from that in complex **2**. The d orbitals should be pushed down for  $\text{Au}^{3+}$  as compared to  $\text{Pt}^{2+}$  for two reasons: the higher nuclear charge sensed by the electrons and the presence of the second electronegative chlorine atom.<sup>109</sup> Consequently, the metal d orbitals should become closer in energy to the ligand orbitals, whose weights in the resulting frontier MOs should increase. Indeed, the metal–chlorine  $\pi$ -antibonding highest occupied MO (HOMO) is centered on the metal much more in the case of **1** than in the case of complex **2**.

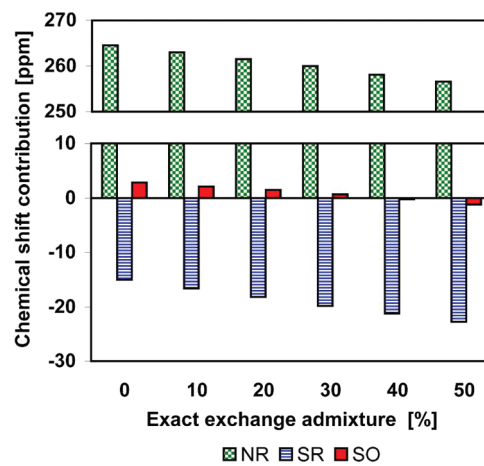


**Figure 9.** NR, SR, and SO contributions to the NMR chemical shift for N-1 in compound **2** calculated by using a PBE0 functional with various amounts of exact exchange.

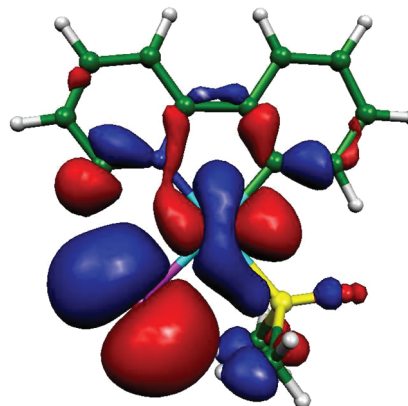


**Figure 10.** The highest MO relevant for the  $\Delta_{\text{SO}}$  contribution to atom N-1 (HOMO-3) in complex **1**.

The contribution of the HOMO to the net Mulliken population of metal d orbitals is as much as 0.39 for Pt and only 0.12 for Au.

For an orbital to be relevant to the  $\Delta_{\text{SO}}$  contribution, it must contain at least some s character from the light atom in question as well as a contribution from the heavy atom. For reasons of symmetry, the highest MO relevant here is the HOMO-3 (MO lying three levels below the HOMO) of complex **1** (Figure 10). Its counterpart in complex **2** is HOMO-2 (Figure 11). The pattern observed here is the same as for the HOMOs: much more metal character in the  $\text{Pt}^{2+}$  than in the  $\text{Au}^{3+}$  complex. In particular, the HOMO-3 of complex **1** contains 28% of the net Pt d and p orbitals and 3% of the net N-1 sp hybrid orbital, whereas the HOMO-2 of complex **2** contains only 12% of the net Au d and p orbitals and 5% of the net N-1 sp hybrid orbital (compare Figures 10 and 11). In both cases, the remainder of the electron density is found mainly in the lone pairs of the one (two) chlorine atom(s). We conclude by stating that the  $\Delta_{\text{SO}}$  for N-1 is much smaller in the  $\text{Au}^{3+}$  complex due to the higher ionicity of the bonding, since the much smaller metal d-orbital character of the relevant MO induces a smaller “spin polarization” within the nitrogen s orbitals. In contrast to the  $\Delta_{\text{SO}}$  for N-1, the  $\Delta_{\text{SO}}$  for C-2' is *not* quenched in the case of  $\text{Au}^{3+}$ , presumably because the relevant MO describing the  $\text{Au}\cdots\text{C-2}'$  bonding

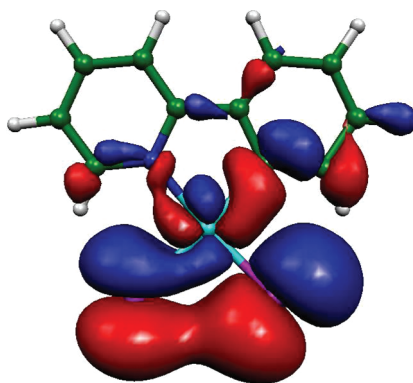


**Figure 11.** The highest MO relevant for the  $\Delta_{\text{SO}}$  contribution to atom N-1 (HOMO-2) in complex 2.

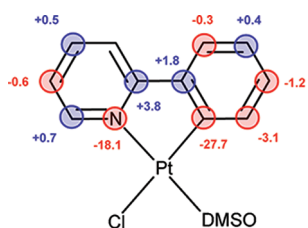


**Figure 12.** SO contributions to the  $^{13}\text{C}$  and  $^{15}\text{N}$  NMR chemical shifts for compound 1.

(HOMO-19, 25% of the net Au s and d population, 3% of the net C-2' sp hybrid orbital) lies much lower in energy than HOMO-2. The different behavior of the SO and SR corrections to the N-1 and C-2' shifts in **1** as compared with **2** might also be related to the fact that the corrections for C-2' originate mainly in the in-plane components of the chemical-shift tensor, but the corrections for N-1 are significantly influenced by the out-of-plane  $\delta_{33}$  component (Table S9, Supporting Information).

The SO contributions to the NMR chemical shifts (Table 4) of the remaining atoms of the aromatic system (Figure 12) are much smaller and, at a first approximation, resemble a “mesomeric effect” spreading from the metal center. The observed trends originate in the propagation of the SO effect via the aromatic system through Fermi-contact (FC) interaction. This propagation resembles the pattern of indirect nuclear spin–spin coupling as has been elegantly demonstrated by Kaupp and co-workers.<sup>110</sup>

**3.2.6. Effects of Geometry.** After finding the optimal method for reproducing the experimental  $^{13}\text{C}$  NMR chemical shifts using the B3LYP geometry, we then adopted an inverse approach: The optimal PBE0(30)/TZP/ZORA-SO/COSMO method for compound **1** was applied to various optimized geometries (BLYP, B3LYP, BH and HLYP, MP2) and to the X-ray geometry with B3LYP optimized hydrogens. The  $^{13}\text{C}$  NMR chemical shifts for the MP2 and X-ray geometries of compound **1** are plotted and compared to experimental NMR data in Figure 13; an analogous comparison is presented for the DFT geometries in Figure S4, Supporting Information.

As our main reference, we again consider the trend in the experimental chemical shifts qualitatively (with the same ordering of carbons according to decreasing chemical shift from theory and experiment) as well as quantitatively (close slopes of the corresponding lines). The PBE0(30)/TZP/ZORA-SO/COSMO approach provides quantitatively correct trends for all carbon

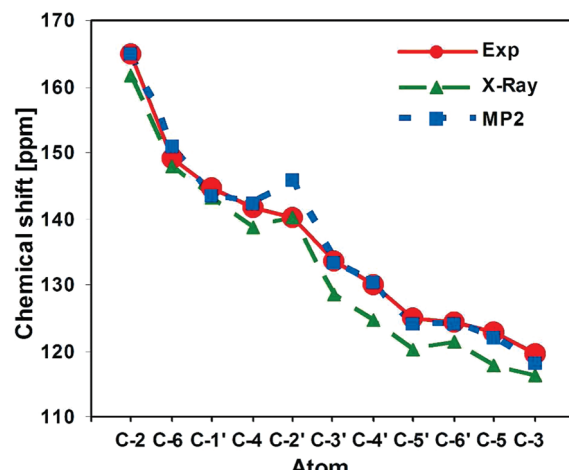


**Figure 13.** Experimental  $^{13}\text{C}$  NMR chemical shifts for compound **1** and those calculated using PBE0(30) for X-ray (with B3LYP optimized protons) and MP2 geometries.

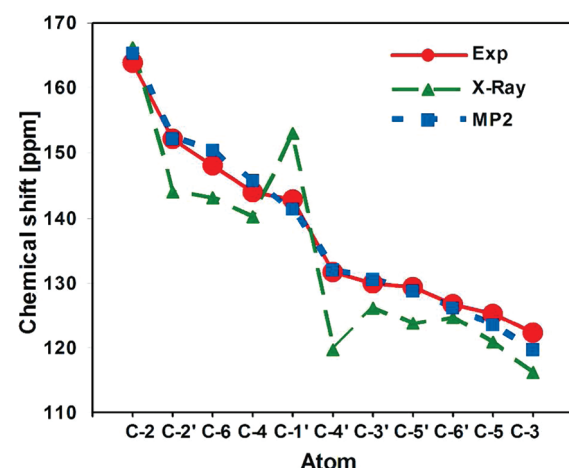


**Figure 14.** Experimental  $^{13}\text{C}$  NMR chemical shifts for compound **2** and those calculated using PBE0(40) for X-ray (with B3LYP optimized hydrogens) and MP2 geometries.

shifts with any of the BLYP, B3LYP, and BH and HLYP structures. The best absolute shifts were found for the B3LYP structure (cf. Figure S4, Supporting Information).

The X-ray structure of **1** provides relatively good agreement with experiment, consistently with a relatively good structural factor. Nevertheless it is less suitable than any of the optimized structures. It overestimates the absolute shieldings for C-3' through C-3, presumably because shorter bond lengths are found within the aromatic rings for the crystal structure than for the optimized geometries. More importantly, the X-ray structure, as well as the MP2 structure, incorrectly describes the qualitative trend between the C-4 and C-2' shifts. Apparently, there is a structural difference between the DFT-optimized structures on the one side and the X-ray and MP2 structures on the other. Indeed, the C-2'-Pt distance is 0.02 Å shorter for the X-ray structure and as much as 0.04 Å shorter for the MP2 structure than what is found by the B3LYP method.

The best absolute shifts were found for the B3LYP structure and, disregarding C-2', also for the MP2 structure. Good quantitative trends were also obtained for the BLYP and BH and HLYP

structures. Since the best agreement with NMR experiment was obtained for the B3LYP geometry, the use of this structure for optimizing the method to calculate NMR chemical shifts proved reasonable, and our approach can be considered to be “self-consistent”. A summary of all of the effects gradually included in the calculations is shown schematically for the B3LYP geometry in Figure S5, Supporting Information.

An analogous study of the influence of the geometry (for the DFT employing only the two hybrid functionals) was performed for compound **2**. The PBE0(40)/TZP/ZORA-SO/COSMO results are shown in Figure 14 and Figure S6, Supporting Information. Obviously, the X-ray structure with B3LYP optimized hydrogens (see Section 2.1) shows a dramatic discrepancy with the experimental results for carbons C-1' and C-4'. The NMR chemical shift of C-1' is too large, whereas that of C-4' is too small. The absolute nuclear shielding is thus underestimated for C-1' and overestimated for C-4'. This is consistent with the type of distortion of the benzene ring present in the X-ray structure as compared to the optimized geometry. The bonds from C-1' are elongated,

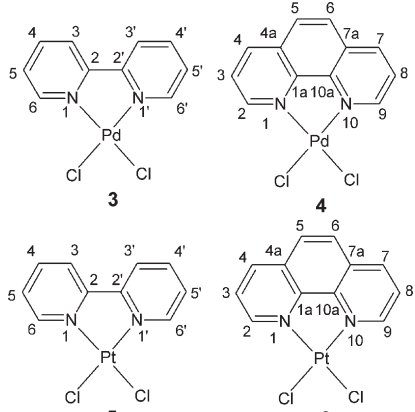
while those from C-4' are shortened. This could also possibly be due to the presence of two slightly shifted positions of the ligand in the crystal, which are, however, averaged to a single set of atomic positions. Since the *R*-factor for this X-ray structure is relatively large and since all optimized structures provide qualitatively correct trends, we conclude that the X-ray structure of **2** is useless for the calculation of the nuclear magnetic shielding in solution.

The best absolute agreement with experiment was obtained for the less shielded atoms C-2 through C-4 with the BHandH-LYP structure (Figure S6, Supporting Information) and for the more shielded atoms C-1' through C-3 with the B3LYP and MP2 geometries. This dependence of the best method for the optimization of structure on the region of shifts in question may be connected to the influence of the solvent: For the most shielded atoms C-5' through C-3, the influence of the COSMO is relatively large. Therefore, an explicit treatment of the solvent, such as a combined molecular dynamics–DFT approach<sup>111–115</sup> (which is beyond the scope of the current contribution) might unify the best structural method for both regions of the shift.

**3.3. Applications to Compounds 3–6.** In addition to **1** and **2**, we tested the “optimized” computational approach on some other compounds shown in Chart 2: **3**, [Pd(bpy)Cl<sub>2</sub>];<sup>116–118</sup> **4**, [Pd(phen)Cl<sub>2</sub>];<sup>116</sup> **5**, [Pt(bpy)Cl<sub>2</sub>];<sup>116,118</sup> and **6**, [Pt(phen)Cl<sub>2</sub>].<sup>116</sup> In the case of Pt and Pd (having the same +2 oxidation state), 30% of the exact exchange admixture for PBE0 functional was applied, whereas for the Au species (+3 oxidation state) we used 40% of the exact exchange admixture. The resulting chemical shifts calculated for compounds **3–6** are summarized in Tables 6 and 7.

It should be noted that while the data for nitrogen and carbon atoms bonded directly to the metal center converge closely to the experimental values when relativistic corrections are applied, the data for carbon atoms more distant from the metal center improve only slightly. In contrast, the NR COSMO data for hydrogen atoms actually deteriorate slightly as compared to the experimental values when relativistic corrections are applied. This deterioration originates, in our opinion, in the insufficient description of the solvation by the implicit solvent model applied here.<sup>119</sup> Applications of the explicit solvent model combining classical molecular

Chart 2. Structures and Atom Numbering for Compounds 3–6<sup>a</sup>



<sup>a</sup>[Pd(bpy)Cl<sub>2</sub>], **3**; [Pd(phen)Cl<sub>2</sub>], **4**; [Pt(bpy)Cl<sub>2</sub>], **5**; and [Pt(phen)Cl<sub>2</sub>], **6**.

Table 6. NMR Chemical Shifts for Compounds **3** and **5** Calculated by ADF using PBE0(30)/TZP/ZORA-SO/COSMO with SR ( $\Delta_{SR}$ ) and SO ( $\Delta_{SO}$ ) Contributions Shown Separately

atom	[Pd(bpy)Cl <sub>2</sub> ], <b>3</b>						[Pt(bpy)Cl <sub>2</sub> ], <b>5</b>					
	$\delta_{NR}^a$	$\Delta_{SR}$	$\delta_{NR}^b + \sigma_{SR}$	$\Delta_{SO}$	$\delta_{NR}^b + \Delta_{SR} + \Delta_{SO}$	expt <sup>e</sup>	$\delta_{NR}^c$	$\Delta_{SR}$	$\delta_{NR}^d + \Delta_{SR}$	$\Delta_{SO}$	$\delta_{NR}^d + \Delta_{SR} + \Delta_{SO}$	expt <sup>e</sup>
N-1	244.8	-5.0	239.8	-20.5	219.3	217.2	243.5	-7.1	236.4	-31.9	204.5	202.1
C-2	156.1	-1.1	155.0	+1.2	156.2	156.8	156.2	-3.7	152.5	+4.7	157.2	157.3
C-3	123.3	-0.3	123.0	-0.1	122.9	124.3	122.9	-1.3	121.6	+1.0	122.6	124.7
C-4	142.0	-0.1	141.9	+0.1	142.0	141.6	141.9	-1.2	140.7	+1.4	142.1	141.0
C-5	127.4	-0.2	127.2	-0.5	126.7	127.7	127.2	-0.6	126.6	+0.1	126.7	128.2
C-6	151.2	-0.5	150.7	-0.6	150.1	150.1	151.2	-2.3	148.9	+0.5	149.4	148.9
RMSD	0.8		1.1		0.8		1.5		2.6		1.3	
H-3	8.14	-0.08	8.06	0.00	8.06	8.58	8.10	+0.08	8.18	-0.20	7.98	8.58
H-4	8.06	+0.07	8.13	-0.14	7.99	8.35	8.08	-0.03	8.05	+0.03	8.08	8.41
H-5	7.47	0.00	7.47	-0.09	7.38	7.80	7.58	+0.02	7.60	-0.09	7.51	7.84
H-6	8.90	-0.04	8.86	-0.06	8.78	9.12	9.15	-0.06	9.09	+0.16	9.25	9.50
RMSD	0.33		0.35		0.42		0.36		0.36		0.40	

<sup>a</sup>ADF/PBE0(30)/TZP/COSMO//G03/B3LYP/ECP28MDF/cc-pwCVTZ-PP+6-31G\*\*/PCM. <sup>b</sup>ADF/PBE0(30)/TZP/ZORA-SO/COSMO//G03/B3LYP/ECP28MDF/cc-pwCVTZ-PP+6-31G\*\*/PCM. <sup>c</sup>ADF/PBE0(30)/TZP/COSMO//G03/B3LYP/ECP60MDF/cc-pwCVTZ-PP+6-31G\*\*/PCM.

<sup>d</sup>ADF/PBE0(30)/TZP/ZORA-SO/COSMO//G03/B3LYP/ECP60MDF/cc-pwCVTZ-PP+6-31G\*\*+/PCM. <sup>e</sup><sup>1</sup>H and <sup>15</sup>N NMR data: Pazderski, L; Szlyk, E; Sitkowski, J; Kamienski, B; Kozerski, L; Tousek, J; Marek, R. *Magn. Reson. Chem.* **2006**, *44*, 163. <sup>13</sup>C NMR data: this work.

**Table 7.** NMR Chemical Shifts for Compounds 4 and 6 Calculated by ADF using PBE(30)/TZP/ZORA-SO/COSMO with SR ( $\Delta_{\text{SR}}$ ) and SO ( $\Delta_{\text{SO}}$ ) Contributions Shown Separately

atom	[Pd(phen)Cl <sub>2</sub> ], 4						[Pt(phen)Cl <sub>2</sub> ], 6					
	$\delta_{\text{NR}}^a$	$\Delta_{\text{SR}}$	$\delta_{\text{NR}}^b + \Delta_{\text{SR}}$	$\Delta_{\text{SO}}$	$\delta_{\text{NR}}^b + \Delta_{\text{SR}} + \Delta_{\text{SO}}$	expt <sup>c</sup>	$\delta_{\text{NR}}^c$	$\Delta_{\text{SR}}$	$\delta_{\text{NR}}^d + \Delta_{\text{SR}}$	$\Delta_{\text{SO}}$	$\delta_{\text{NR}}^d + \Delta_{\text{SR}} + \Delta_{\text{SO}}$	expt <sup>c</sup>
N-1	241.8	-7.0	238.8	-22.0	216.8	215.4	240.2	-8.4	231.8	-30.5	201.3	200.0
C-2	151.3	-0.4	150.9	-0.8	150.1	149.6	151.5	-2.1	149.4	+0.5	149.9	150.5
C-3	125.6	-0.1	125.5	-0.7	124.8	126.4	125.8	-0.7	125.1	-0.2	124.9	126.3
C-4	141.7	-0.1	141.6	+0.2	141.8	139.9	141.4	-1.2	140.2	+1.6	141.8	140.4
C-5	127.7	-0.2	127.5	+0.1	127.6	128.1	127.4	-0.8	126.6	+0.9	127.5	/127.8
C-1a	145.7	-1.0	144.7	+1.4	146.1	148.6	146.0	-3.6	142.4	+5.2	147.6	147.2
C-4a	129.9	-0.2	129.7	0.0	129.7	131.0	129.9	-1.3	128.6	+1.1	129.7	130.9
RMSD	1.0		1.3		1.2		1.6		2.8		1.1	
H-2	9.16	-0.04	9.12	-0.10	9.02	9.34	9.40	-0.06	9.34	+0.01	9.35	9.69
H-3	7.90	-0.01	7.91	-0.08	7.83	8.13	7.95	+0.04	7.99	-0.10	7.89	8.17
H-4	8.70	-0.01	8.69	0.00	8.69	8.97	8.71	-0.04	8.67	-0.02	8.69	9.04
H-5	8.14	0.00	8.14	-0.05	8.09	8.28	8.15	-0.01	8.16	-0.07	8.09	8.29
RMSD	0.21		0.22		0.28		0.26		0.28		0.30	

<sup>a</sup> ADF/PBE0(30)/TZP/COSMO//G03/B3LYP/ECP28MDF/cc-pwCVTZ-PP+6-31G\*\*/PCM. <sup>b</sup> ADF/PBE0(30)/TZP/ZORA-SO/COSMO//G03/B3LYP/ECP28MDF/cc-pwCVTZ-PP+6-31G\*\*/PCM. <sup>c</sup> ADF/PBE0(30)/TZP/COSMO//G03/B3LYP/ECP60MDF/cc-pwCVTZ-PP+6-31G\*\*/PCM. <sup>d</sup> ADF/PBE0(30)/TZP/ZORA-SO/COSMO//G03/B3LYP/ECP60MDF/cc-pwCVTZ-PP+6-31G\*\*/PCM. <sup>e</sup> <sup>1</sup>H and <sup>15</sup>N NMR data: Pazderski, L.; Szlyk, E.; Sitkowski, J.; Kamienski, B.; Kozerski, L.; Tousek, J.; Marek, R. *Magn. Reson. Chem.* 2006, 44, 163. <sup>13</sup>C NMR data: this work.

dynamics and relativistic quantum chemical calculations of NMR chemical shifts<sup>120,121</sup> will be a topic of our future studies. Neglected rovibrational corrections, another possible source of the deviations in the dominant NR part, are expected to play a less significant role because they will, to a large extent, cancel out in the NMR chemical shift calculations.<sup>122</sup>

#### 4. CONCLUSIONS

There are always two sources of uncertainty in any quantum chemical study that aims to reproduce and predict spectroscopic parameters: a sufficiently precise structure and a sufficiently precise computational method for the spectroscopy. Our study suggests that in cases where the experimental data map the compound globally and thus provide topological trends for the observed property the comparison of theory and experiment can help to identify the proper structure.

More general conclusions can be drawn for the hierarchy of physical effects that influence the value of the NMR chemical shift. First, the quantitatively most important (tenths of ppm) effect comes from inclusion of the relativistic corrections with their magnitudes, however, strongly dependent on the amount of the exact exchange in the density functional. Second is the proper choice of geometry: using a poorly resolved X-ray structure (as in the case of compound 2) can result in errors of as much as 15 ppm. The choice of the various theoretical optimizations (BLYP, B3LYP, BH and HLYP, MP2) results in a variation of about 5 ppm, which for the three DFT approaches represents only an incremental shift with all of the nuclear shielding trends preserved. Third in importance is the effect of the continuum solvent model (up to 4 ppm), and last is the decontraction and augmentation of the IGLO-III basis set (up to 2.5 ppm).

Another point of general interest which should be highlighted here arises from the interpretation part. The SO contribution to the nuclear magnetic shielding can be rationalized in terms of the composition of those frontier canonical Kohn–Sham orbitals that have a substantial contribution of s character from the light atom in question as well as a contribution from the heavy atom.

Coming to system-specific conclusions, two X-ray geometries and a series of ab initio structures of six Pd<sup>2+</sup>, Pt<sup>2+</sup>, or Au<sup>3+</sup> complexes were tested on the basis of theoretical vs experimental <sup>13</sup>C NMR chemical shifts, starting with the evaluation of the NMR approach for a certain geometry and then checking the optimal NMR approach back against various structures. Our calculations demonstrate that the B3LYP method with small-core ECPs and the cc-pwCVTZ-PP/6-31G\*\* basis set augmented with PCM embedding provides geometries for complexes 1–6 which are suitable for calculating <sup>13</sup>C chemical shifts very close to the experimental values in terms of both the trends and the absolute values. The same is true for the MP2 method tested on complexes 1 and 2, with the exception of the chemical shift of C-2' in 1. Good quantitative trends with offsets of the <sup>13</sup>C chemical shifts ranging from about +3 ppm to about -3 ppm were also obtained for the BLYP structures (the shifts were overestimated in complex 1) and BH and HLYP structures (the shifts were underestimated in complexes 1 and 2). The relatively well-resolved X-ray structure of 1 provides correct qualitative trends, except for the chemical shift of C-2', with individual offsets between 0 and -5 ppm; it can therefore be used for qualitative NMR predictions. In contrast, the insufficiently resolved or conformation-averaged X-ray structure of 2 predicts qualitatively incorrect shifts for C-1' and C-4', related to the distortion of the C-1'–C6' aromatic ring. Thus it cannot be used to calculate quantitative NMR data in solution.

Evaluating the approaches for calculating the chemical shift, the most strongly method-dependent term is the largely negative SO contribution to the chemical shifts of C-2' and N-1. Increasing the amount of the exact exchange from 0 to 50% makes the SO contribution more than 10 ppm more negative for C-2' of 2 and N-1 of 1 and by more than 20 ppm for C-2' of 1. The total SO contributions for these atoms vary from about -5 ppm to -40 ppm. The situation is completely different for N-1 of 2, where the SO contribution amounts to 0 ± 3 ppm for any of the exact exchange admixtures. We interpret this finding on the basis of the much more

ionic character of the bonding in the  $\text{Au}^{3+}$  system as compared to the  $\text{Pt}^{2+}$  complex.

If the SO contributions are less important and less method-dependent in the  $\text{Au}^{3+}$  as compared to the  $\text{Pt}^{2+}$  complex, the opposite is true for the SR term. The SR term, which is described equally well by the relativistic ECPs and the ZORA, is again largest for C-2' and N-1 (about  $-10$  ppm in **1**, between  $-20$  and  $-30$  ppm in **2**). However, the SO and SR terms are also sizable ( $\pm 3$  to  $\pm 5$  ppm) for the atoms separated from the metal by two bonds (C-2, C-1', and C-3'), although they partially compensate for each other. The always positive NR chemical shift for the C-2' and N-1 atoms of both **1** and **2** decreases moderately (0 to 8 ppm) upon going from 0% to 50% of the exact exchange admixture.

Adding the SO, SR, and NR terms together and comparing the total chemical shift with the experimental results, we can tune the optimum amount of the exact exchange in the B3LYP or PBE0 density functional. The latter comes out differently for the Pt complex **1** (30%) than for the Au complex **2** (40–50%). This finding, not uncommon in the literature, enables a “pragmatic choice” of the density functional; it is however unsatisfactory from the theoretical point of view. These complexes can thus be suggested as test examples for local hybrid functionals that tune the exact exchange internally. Their development is motivated by a need for a uniform approach to the various systems.<sup>123–125</sup>

## ■ ASSOCIATED CONTENT

**S Supporting Information.** Interatomic distances around the gold center for compound **2**; experimental  $^{13}\text{C}$  NMR chemical shifts for compound **1** and those calculated by using BLYP, BP86, and PW91 for B3LYP-optimized geometry and KT1, KT2, and PBE0(30) for B3LYP-optimized geometry; experimental  $^{13}\text{C}$  NMR chemical shifts for compound **1** and those calculated using PBE0(30) for selected DFT geometries (BLYP, B3LYP, BHandHLYP); experimental  $^{13}\text{C}$  NMR chemical shifts for compound **1** and those calculated using PBE0(30) incorporating various physical effects; experimental  $^{13}\text{C}$  NMR chemical shifts for compound **2** and those calculated using PBE0(40) for selected DFT geometries (B3LYP, BHandHLYP); selected interatomic distances obtained by using various optimization approaches; NR NMR chemical shifts for compound **1**; SR NMR chemical shifts for compound **1**; NMR chemical shifts for compound **1** obtained from the ADF program using ZORA-SO and functionals VWN, PW92, BP86, PW91, BLYP, B3LYP, BHandHLYP; NMR chemical shifts for compounds **1** and **2** calculated by ADF/B3LYP/TZP/ZORA-SO/COSMO and ADF/PBE0/TZP/ZORA-SO/COSMO with a varying (0–50%) exact exchange admixture parameter; NR, SR, and SO contributions to the principal components of the NMR chemical shift tensor for compounds **1** and **2**; NR, SR, and SO contributions to the NMR chemical shifts for compounds **1** and **2** calculated by ADF/TZP/ZORA-SO/COSMO with a varying (0–50%) exact exchange admixture; and atomic coordinates for all systems employed in this study. This material is available free of charge via the Internet at <http://pubs.acs.org>.

## ■ AUTHOR INFORMATION

### Corresponding Author

\*E-mail: marketa@ncbr.chemi.muni.cz; rmarek@chemi.muni.cz.

### Notes

The authors declare no competing financial interest.

## ■ ACKNOWLEDGMENT

We thank Stanislav Standara (Brno) and Juha Vaara (Oulu) for providing the Fægri-III basis set for platinum and gold and Michal Straka (Prague), Martin Kaupp (Berlin), and Jaromír Marek (Brno) for several helpful discussions. We also would like to thank reviewers for their valuable comments. The authors gratefully acknowledge the financial support of the Ministry of Education of the Czech Republic (grants MSM0021622413 and LC06030 to MM and RM), the project “CEITEC – Central European Institute of Technology” (CZ.1.05/1.1.00/02.0068) from the European Regional Development Fund, and the Erasmus LLP program (T.P. study stay at Masaryk University). The computational resources were partly provided by Meta-Centrum, Czech Republic (grant MSM6383917201).

## ■ REFERENCES

- (1) *Metal ions in biological systems*; Sigel, A., Sigel, H., Eds; Marcel Dekker, Inc.: New York, 1996; Vol. 33, pp 269–675.
- (2) Orvig, C.; Abrams, M. *J. Chem. Rev.* **1999**, *99*, 2201–2204.
- (3) Messori, L.; Abbate, F.; Marcon, G.; Orioli, P.; Fontani, M.; Mini, E.; Mazzei, T.; Carotti, S.; O’Connell, T.; Zanello, P. *J. Med. Chem.* **2000**, *43*, 3541–3548.
- (4) Okada, T.; El-Mehasseb, I. M.; Kodaka, M.; Tomohiro, T.; Okamoto, K. I.; Okuno, H. *J. Med. Chem.* **2001**, *44*, 4661–4667.
- (5) El-Mehasseb, I. M.; Kodaka, M.; Okada, T.; Tomohiro, T.; Okamoto, K.; Okuno, H. *J. Inorg. Biochem.* **2001**, *84*, 157–158.
- (6) Edwards, G. L.; Black, D. S. C.; Deacon, G. B.; Wakelin, L. P. G. *Can. J. Chem.* **2005**, *83*, 980–989.
- (7) Edwards, G. L.; Black, D. S. C.; Deacon, G. B.; Wakelin, L. P. G. *Can. J. Chem.* **2005**, *83*, 969–979.
- (8) Parish, R. V.; Howe, B. P.; Wright, J. P.; Mack, J.; Pritchard, R. G.; Buckley, R. G.; Elsome, A. M.; Fricker, S. P. *Inorg. Chem.* **1996**, *35*, 1659–1666.
- (9) Fan, D.; Yang, C. T.; Ranford, J. D.; Lee, P. F.; Vittal, J. J. *Dalton Trans.* **2003**, 2680–2685.
- (10) Henderson, W.; Nicholson, B. K.; Faville, S. J.; Fan, D.; Ranford, J. D. *J. Organomet. Chem.* **2001**, *631*, 41–46.
- (11) Fan, D.; Yang, C. T.; Ranford, J. D.; Vittal, J. J.; Lee, P. F. *Dalton Trans.* **2003**, 3376–3381.
- (12) Lo, V. K. Y.; Kung, K. K. Y.; Wong, M. K.; Che, C. M. *J. Organomet. Chem.* **2009**, *694*, 583–591.
- (13) Beletskaya, I. P.; Kashin, A. N.; Karlstedt, N. B.; Mitin, A. V.; Cheprakov, A. V.; Kazankov, G. M. *J. Organomet. Chem.* **2001**, *622*, 89–96.
- (14) Schnyder, A.; Indolese, A. F.; Studer, M.; Blaser, H. U. *Angew. Chem., Int. Ed.* **2002**, *41*, 3668–3671.
- (15) Del Zotto, A.; Prat, F. I.; Baratta, W.; Zangrando, E.; Rigo, P. *Inorg. Chim. Acta* **2009**, *362*, 97–104.
- (16) Atla, S. B.; Kelkar, A. A.; Puranik, V. G.; Bensch, W.; Chaudhari, R. V. *J. Organomet. Chem.* **2009**, *694*, 683–690.
- (17) *Two-Dimensional NMR spectroscopy*; Croasmun, W. R., Carlson, R. M. K., Eds.; VCH: New York, 1994; pp 619–914.
- (18) Ranconi, L.; Sadler, P. J. *Coord. Chem. Rev.* **2008**, *252*, 2239–2277.
- (19) *Calculation of NMR and EPR Parameters. Theory and Application*; Kaupp, M., Bühl, M., Malkin, V. G., Eds.; Wiley-VCH: Weinheim, Germany, 2004; pp 153–277.
- (20) Vaara, J. *Phys. Chem. Chem. Phys.* **2007**, *9*, 5399–5418.
- (21) Solomon, E. I.; Scott, R. A.; King, R. B. *Computational Inorganic and Bioinorganic Chemistry*; John Wiley & Sons: Singapore, 2009, 55–107.
- (22) Pyykkö, P. Theory of NMR parameters. From Ramsey to relativity, 1953–1983. In *Calculation of NMR and EPR Parameters. Theory and Application*; Kaupp, M., Bühl, M.; Malkin, V. G., Eds.; Wiley-VCH: Weinheim, Germany, 2004; pp 7–19.
- (23) Pyykkö, P. *Chem. Rev.* **1988**, *88*, 563–594.
- (24) Malkin, V. G.; Malkina, O. L.; Reviakine, R.; Arbuznikov, A. V.; Kaupp, M.; Schimmpfennig, B.; Malkin, I.; Repisky, M.; Komorovsky,

- S.; Hrobarik, P.; Malkin, E.; Helgaker, T.; Ruud, K. *MAG-ReSpect*, version 2.3; Universität Würzburg: Würzburg, Germany, 2010.
- (25) With new contributions from: Saue, T.; Visscher, L.; Jensen, H. J. Aa.; Bast, R.; Dyall, K. G.; Ekström, U.; Eliav, E.; Enevoldsen, T.; Fleig, T.; Gomes, A. S. P.; Henriksson, J.; Ilias, M.; Jacob, C. R.; Knecht, S.; Nataraj, H. S.; Norman, P.; Olsen, J.; Pernpointner, M.; Ruud, K.; Schimmelpfennig, B.; Sikkema, J.; Thorvaldsen, A.; Thyssen, J.; Villaume, S.; Yamamoto, S. *DIRAC, a relativistic ab initio electronic structure program*, release DIRAC10; University of Souther Denmark: Odense M, Denmark, 2010.
- (26) Hrobárik, P.; Hrobáriková, V.; Meier, F.; Repíský, M.; Komorovský, S.; Kaupp, M. *J. Phys. Chem. A* **2011**, *115*, 5654–5659.
- (27) Vaara, J.; Manninen, P.; Lantto, P. Perturbational and E. C. P. Calculation of Relativistic Effects in NMR Shielding and Spin–Spin Coupling. In *Calculation of NMR and EPR Parameters. Theory and Application*; Kaupp, M., Bühl, M., Malkin, V. G., Eds; Wiley-VCH: Weinheim, Germany, 2004, pp 209–226.
- (28) Guerra, C. F.; Snijders, J. G.; te Velde, G.; Baerends, E. J. *Theor. Chem. Acc.* **1998**, *99*, 391–403.
- (29) Van Lenthe, E.; Baerends, E. J.; Snijders, J. G. *J. Chem. Phys.* **1993**, *101*, 9783–9792.
- (30) Wolff, S. K.; Ziegler, T.; van Lenthe, E.; Baerends, E. J. *J. Chem. Phys.* **1999**, *110*, 7689–7698.
- (31) van Lenthe, E.; Ehlers, A. E.; Baerends, E. J. *J. Chem. Phys.* **1999**, *110*, 8943–8953.
- (32) van Lenthe, E.; Snijders, J. G.; Baerends, E. J. *J. Chem. Phys.* **1996**, *105*, 6505–6516.
- (33) Krykunov, M.; Ziegler, T.; van Lenthe, E. *J. Phys. Chem. A* **2009**, *113*, 11495–11500.
- (34) Godbert, N.; Pugliese, T.; Aiello, I.; Bellusci, A.; Crispini, A.; Ghedini, M. *Eur. J. Inorg. Chem.* **2007**, *2007*, 5105–5111.
- (35) Kobayashi, M.; Masaoka, S.; Sakai, K. *Acta Crystallogr. E* **2008**, *64*, M1325–U3003.
- (36) Pazderski, L.; Pawlak, T.; Sitkowski, J.; Kozerski, L.; Szlyk, E. *Magn. Reson. Chem.* **2009**, *47*, 932–941.
- (37) Craig, C. A.; Garces, F. O.; Watts, R. J.; Palmans, R.; Frank, A. J. *Coord. Chem. Rev.* **1990**, *97*, 193–208.
- (38) Frisch, M. J.; Trucks, G. W.; Schlegel, H. B.; Scuseria, G. E.; Robb, M. A.; Cheeseman, J. R.; Montgomery, J. A. Jr.; Vreven, T.; Kudin, K. N.; Burant, J. C.; Millam, J. M.; Iyengar, S. S.; Tomasi, J.; Barone, V.; Mennucci, B.; Cossi, M.; Scalmani, G.; Rega, N.; Petersson, G. A.; Nakatsuji, H.; Hada, M.; Ehara, M.; Toyota, K.; Fukuda, R.; Hasegawa, J.; Ishida, M.; Nakajima, T.; Honda, Y.; Kitao, O.; Nakai, H.; Klene, M.; Li, X.; Knox, J. E.; Hratchian, H. P.; Cross, J. B.; Bakken, V.; Adamo, C.; Jaramillo, J.; Gomperts, R.; Stratmann, R. E.; Yazyev, O.; Austin, A. J.; Cammi, R.; Pomelli, C.; Ochterski, J. W.; Ayala, P. Y.; Morokuma, K.; Voth, G. A.; Salvador, P.; Dannenberg, J. J.; Zakrzewski, V. G.; Dapprich, S.; Daniels, A. D.; Strain, M. C.; Farkas, O.; Malick, D. K.; Rabuck, A. D.; Raghavachari, K.; Foresman, J. B.; Ortiz, J. V.; Cui, Q.; Baboul, A. G.; Clifford, S.; Cioslowski, J.; Stefanov, B. B.; Liu, G.; Liashenko, A.; Piskorz, P.; Komaromi, I.; Martin, R. L.; Fox, D. J.; Keith, T.; Al-Laham, M. A.; Peng, C. Y.; Nanayakkara, A.; Challacombe, M.; Gill, P. M. W.; Johnson, B.; Chen, W.; Wong, M. W.; Gonzalez, C.; Pople, J. A. Gaussian, Inc., *Gaussian 03*, revision E.01; Gaussian, Inc.: Wallingford, CT, 2004.
- (39) Baerends, E. J.; Autschbach, J.; Bashford, D.; Bérces, A.; Bickelhaupt, F. M.; Bo, C.; Boerriger, P. M.; Cavallo, L.; Chong, D. P.; Deng, L.; Dickson, R. M.; Ellis, D. E.; van Faassen, M.; Fan, L.; Fischer, T. H.; Fonseca Guerra, C.; Ghysels, A.; Giammona, A.; van Gisbergen, S. J. A.; Götz, A. W.; Groeneveld, J. A.; Gritsenko, O. V.; Grüning, M.; Harris, F. E.; van den Hoek, P.; Jacob, C. R.; Jacobsen, H.; Jensen, L.; van Kessel, G.; Kootstra, F.; Krykunov, M. V.; van Lenthe, E.; McCormack, D. A.; Michalak, A.; Mitoraj, M.; Neugebauer, J.; Nicu, V. P.; Noodleman, L.; Osinga, V. P.; Patchkovskii, S.; Philipsen, P. H. T.; Post, D.; Pye, C. C.; Ravenek, W.; Rodríguez, J. I.; Ros, P.; Schipper, P. R. T.; Schreckenbach, G.; Seth, M.; Snijders, J. G.; Solà, M.; Swart, M.; Swerhone, D.; te Velde, G.; Vernooij, P.; Versluis, L.; Visscher, L.; Visser, O.; Wang, F.; Wesolowski, T. A.; van Wezenbeek, E. M.; Wiesenecker, G.; Wolff, S. K.; Woo, T. K.; Yakovlev, A. L.; Ziegler, T. *ADF2009.01*; SCM: Amsterdam, The Netherlands.
- (40) Godbert, N.; Pugliese, T.; Aiello, I.; Bellusci, A.; Crispini, A.; Ghedini, M. *Eur. J. Inorg. Chem.* **2007**, *5105–5111*.
- (41) Maekawa, M.; Munakata, M.; Kitagawa, S.; Nakamura, M. *Anal. Sci.* **1991**, *7*, 521–522.
- (42) Osborn, R. S.; Rogers, D. *J. Chem. Soc., Dalton Trans.* **1974**, 1002–1004.
- (43) Groom, C. R.; Allen, F. H. *WIREs Comput. Mol. Sci.* **2011**, *1*, 368–376.
- (44) Roothaan, C. C. *J. Rev. Mod. Phys.* **1951**, *23*, 69–89.
- (45) Pople, J. A.; Nesbet, R. K. *J. Chem. Phys.* **1954**, *22*, 571–572.
- (46) Moller, C.; Plesset, M. S. *Phys. Rev.* **1934**, *46*, 618–622.
- (47) Head-Gordon, M.; Pople, J. A.; Frisch, M. J. *Chem. Phys. Lett.* **1988**, *153*, 503–506.
- (48) Lee, C.; Yang, W.; Parr, R. G. *Phys. Rev. B* **1988**, *37*, 785–789.
- (49) Becke, A. D. *Phys. Rev. A* **1988**, *38*, 3098–3100.
- (50) Becke, A. D. *J. Chem. Phys.* **1993**, *98*, 5648–5652.
- (51) Becke, A. D. *J. Chem. Phys.* **1993**, *98*, 1372–1377.
- (52) Koch, W.; Holthausen, M. C. *A Chemist's Guide to Density Functional Theory*; Wiley-VCH: Wenheim, Germany, 2000; pp 119–136.
- (53) Figgen, D.; Peterson, K. A.; Dolg, M.; Stoll, H. *J. Chem. Phys.* **2009**, *130*, 164108.
- (54) Wood, J. H.; Boring, A. M. *Phys. Rev. B* **1978**, *18*, 2701–2711.
- (55) Andrae, D.; Haeussermann, U.; Dolg, M.; Stoll, H.; Preuss, H. *Theor. Chim. Acta* **1990**, *77*, 123–141.
- (56) Martin, J. M. L.; Sundermann, A. *J. Chem. Phys.* **2001**, *114*, 3408–3420.
- (57) Hay, P. J.; Wadt, W. R. *J. Chem. Phys.* **1985**, *82*, 270–283.
- (58) Wadt, W. R.; Hay, P. J. *J. Chem. Phys.* **1985**, *82*, 284–298.
- (59) Hay, P. J.; Wadt, W. R. *J. Chem. Phys.* **1985**, *82*, 299–310.
- (60) Hariharan, P. C.; Pople, J. A. *Theor. Chim. Acta* **1973**, *28*, 213–222.
- (61) Franci, M. M.; Petro, W. J.; Hehre, W. J.; Binkley, J. S.; Gordon, M. S.; DeFrees, D. J.; Pople, J. A. *J. Chem. Phys.* **1982**, *77*, 3654–3665.
- (62) Krishnan, R.; Binkley, J. S.; Seeger, R.; Pople, J. A. *J. Chem. Phys.* **1980**, *72*, 650–654.
- (63) Miertuš, S.; Scrocco, E.; Tomasi, J. *Chem. Phys.* **1981**, *55*, 117–129.
- (64) Tomasi, J.; Mennucci, B.; Cammi, R. *Chem. Rev.* **2005**, *105*, 2999–3094.
- (65) Bodenhausen, G.; Ruben, D. *J. Chem. Phys. Lett.* **1980**, *69*, 185–189.
- (66) Bax, A.; Summers, M. F. *J. Am. Chem. Soc.* **1986**, *108*, 2083–2084.
- (67) Willker, W.; Leibfritz, D.; Kerssebaum, R.; Bermel, W. *Magn. Reson. Chem.* **1993**, *31*, 287–292.
- (68) Marek, R.; Lyčka, A. *Curr. Org. Chem.* **2002**, *6*, 35–66.
- (69) Marek, R.; Lyčka, A.; Kolehmainen, E.; Sievänen, E.; Toušek, J. *Curr. Org. Chem.* **2007**, *11*, 1154–1205.
- (70) London, F. *J. Phys. Radium* **1937**, *8*, 397–409.
- (71) Pople, J. A. *Proc. R. Soc London* **1957**, *239*, 541–549.
- (72) Pople, J. A. *Proc. R. Soc London* **1957**, *239*, 550–556.
- (73) Pedrew, J. P. *Phys. Rev. B* **1986**, *33*, 8822–8824.
- (74) Pedrew, J. P. *Phys. Rev. B* **1986**, *34*, 7406–7406.
- (75) Perdew, J. P. In *Electronic Structure of Solids '91*; Ziesche, P., Eschring, H., Eds.; Akademie Verlag: Berlin, Germany, 1991; pp 11–20.
- (76) Burke, K.; Perdew, J. P.; Wang, Y. In *Electronic Density Functional Theory. Recent Progress and New Directions*; Dobson, J. F., Vignale, G., Das, M. P., Eds.; Plenum Press: New York, 1998; pp 81–111.
- (77) Perdew, J. P.; Wang, Y. *Phys. Rev. B* **1992**, *45*, 13244–13249.
- (78) Perdew, J. P.; Ernzerhof, M.; Burke, K. *J. Chem. Phys.* **1996**, *105*, 9982–9985.
- (79) Burke, K.; Ernzerhof, M.; Perdew, J. P. *Chem. Phys. Lett.* **1997**, *265*, 115–120.
- (80) Manninen, P.; Lantto, P.; Vaara, J.; Ruud, K. *J. Chem. Phys.* **2003**, *119*, 2623–2637.
- (81) Manninen, P.; Ruud, K.; Lantto, P.; Vaara, J. *J. Chem. Phys.* **2005**, *122*, 114107.
- (82) Fægri, K., Jr.; Almlöf, J. *J. Comput. Chem.* **1986**, *7*, 396–405.

- (83) Kutzelnigg, W.; Fleischer, U.; Schindler, M. In *NMR Basic Principles and Progress*; Diehl, P., Fluck, E., Günther, H., Kosfeld, R., Seelig, J., Eds.; Springer-Verlag: Berlin, Germany, 1990; Vol. 23, pp 165–262.
- (84) Parr, R. G.; Yang, W. *Density-Functional Theory of Atoms and Molecules*; Oxford University Press: Oxford, 1994, pp 152–157.
- (85) Perdew, J. P.; Wang, Y. *Phys. Rev. B* **1992**, *45*, 13244–13249.
- (86) Vosko, S. H.; Wilk, L.; Nusair, M. *Can. J. Phys.* **1980**, *58*, 1200–1211.
- (87) Keal, T. W.; Tozer, D. J. *J. Chem. Phys.* **2003**, *119*, 3015–3024.
- (88) Mennucci, B.; Tomasi, J. *J. Chem. Phys.* **1997**, *106*, 5151–5158.
- (89) Klamt, A.; Schuurmann, G. *J. Chem. Soc., Perkin Trans. 2* **1993**, *799*–805.
- (90) Pye, C. C.; Ziegler, T. *Theor. Chem. Acc.* **1999**, *101*, 396–408.
- (91) van Wuellen, C. *Phys. Chem. Chem. Phys.* **2000**, *2*, 2137–2144.
- (92) Standara, S.; Bouzková, K.; Straka, M.; Zacharová, Z.; Hocek, M.; Marek, J.; Marek, R. *Phys. Chem. Chem. Phys.* **2011**, *13*, 15854–15864.
- (93) Flukiger, P.; Portmann, S. *MOLEKEL 4.3*; Swiss Center for Scientific Computing: Manno, Switzerland, 2002.
- (94) Jonas, V.; Thiel, W. *J. Chem. Phys.* **1995**, *102*, 8474–8484.
- (95) Pazderski, L.; Tousek, J.; Sitkowski, J.; Kozerski, L.; Szlyk, E. *Magn. Reson. Chem.* **2007**, *45*, 1045–1058.
- (96) Travnicek, Z.; Popa, I.; Cajan, M.; Herchel, R.; Marek, J. *Polyhedron* **2007**, *26*, S271–S282.
- (97) Leininger, T.; Nicklass, A.; Kuchle, W.; Stoll, H.; Dolg, M.; Bergner, A. *Chem. Phys. Lett.* **1996**, *255*, 274–280.
- (98) Straka, M.; Kaupp, M. *Chem. Phys.* **2005**, *311*, 45–56.
- (99) Huzinaga, S. *Approximate Atomic Functions*, University of Alberta: Edmonton, Canada, 1971.
- (100) Jensen, F. *Introduction to Computational Chemistry*, 1st ed.; Wiley & Sons Ltd.: Chichester, U.K., 1999; p 155.
- (101) *Extensible Computational Chemistry Environment Basis Set Database*, version 1.2.2; Molecular Science Computing Facility, Pacific Northwest Laboratory: Richland, WA.
- (102) Jensen, F. *J. Chem. Theory Comput.* **2008**, *4*, 719–727.
- (103) Malkin, V. G.; Malkina, O. L.; Salahub, D. R. *Chem. Phys. Lett.* **1996**, *261*, 335–345.
- (104) Kaupp, M.; Malkina, O. L.; Malkin, V. G. *Chem. Phys. Lett.* **1997**, *265*, 55–59.
- (105) Wolff, S. K.; Ziegler, T. *J. Chem. Phys.* **1998**, *109*, 895–905.
- (106) Gilbert, T. M.; Ziegler, T. *J. Phys. Chem. A* **1999**, *103*, 7535–7543.
- (107) Bühl, M. *Chem. Phys. Lett.* **1997**, *267*, 251–257.
- (108) Munzarová, M.; Kaupp, M. *J. Phys. Chem. A* **1999**, *103*, 9966–9983.
- (109) Albright, T. A.; Burdett, J. K.; Whangbo, M.-H. *Orbital Interactions in Chemistry*; Wiley & Sons, Inc.: New York, 1985; pp 82 and 145.
- (110) Kaupp, M.; Malkina, O. L.; Malkin, V. G.; Pyykkö, P. *Chem.—Eur. J.* **1998**, *4*, 118–126.
- (111) Malkin, V. G.; Malkina, O. L.; Steinebrunner, G.; Huber, H. *Chem.—Eur. J.* **1996**, *2*, 452–457.
- (112) Pennanen, T. S.; Vaara, J.; Lantto, P.; Sillanpää, A. J.; Laasonen, K.; Jokisaari, J. *J. Am. Chem. Soc.* **2004**, *126*, 11093–11102.
- (113) Bühl, M.; Grigoleit, S.; Kabrede, H.; Mauschick, F. T. *Chem.—Eur. J.* **2005**, *12*, 477–488.
- (114) Asher, J. R.; Doltsinis, N. L.; Kaupp, M. *J. Am. Chem. Soc.* **2004**, *126*, 9854–9861.
- (115) Přecechtělová, J.; Novák, P.; Munzarová, M. L.; Kaupp, M.; Sklenář, V. *J. Am. Chem. Soc.* **2010**, *132*, 17139–17148.
- (116) Pazderski, L.; Szlyk, E.; Sitkowski, J.; Kamienski, B.; Kozerski, L.; Tousek, J.; Marek, R. *Magn. Reson. Chem.* **2006**, *44*, 163–170.
- (117) Maekawa, M.; Munakata, M.; Kitagawa, S.; Nakamura, M. *Anal. Sci.* **1991**, *7*, 521–522.
- (118) Carty, A. J.; Skeleton, B. W.; Traill, P. R.; White, A. H. *Aust. J. Chem.* **1992**, *45*, 417–422.
- (119) Dračinský, M.; Bouř, P. *J. Chem. Theory Comput.* **2010**, *6*, 288–299.
- (120) Standara, S.; Kulhánek, P.; Marek, R.; Horníček, J.; Bouř, P.; Straka, M. *Theor. Chem. Acc.* **2011**, *129*, 677–684.
- (121) Truflandier, L. A.; Autschbach, J. *J. Am. Chem. Soc.* **2010**, *132*, 3472–3483.
- (122) Vaara, J.; Lounila, J.; Ruud, K.; Helgaker, T. *J. Chem. Phys.* **1998**, *109*, 8388–8396.
- (123) Kaupp, M.; Arbuznikov, A.; Bahmann, H. *Zeitschr. Phys. Chem.* **2010**, *224*, 545–568.
- (124) Arbuznikov, A. V.; Kaupp, M. *J. Chem. Phys.* **2009**, *131*, 084103.
- (125) Arbuznikov, A. V.; Kaupp, M. *Chem. Phys. Lett.* **2007**, *440*, 160–168.